



## Sedimentary pigments reveal complex ecosystem responses of primary producers to mid-Holocene summer anoxia in a small Greenland lake

Mia T. Tuccillo<sup>a,\*</sup>, Shayna C. Garla<sup>b</sup>, Magdalena R. Osburn<sup>a</sup>, Bailey C. Nash<sup>a</sup>, Yarrow Axford<sup>a</sup>

<sup>a</sup> Department of Earth, Environmental & Planetary Sciences, Northwestern University, Evanston, IL, USA

<sup>b</sup> Department of Earth & Environmental Sciences, Syracuse University, Syracuse, NY, USA

### ARTICLE INFO

Handling Editor: Dr P Rioual

**Keywords:**  
 Pigments  
 Paleolimnology  
 Paleoclimate  
 Greenland  
 Arctic  
 Primary productivity  
 Anoxia  
 Holocene

### ABSTRACT

Freshwater ecosystems in the Arctic are particularly sensitive to climate change, and current anthropogenic warming has demonstrably influenced Arctic lake productivity. Paleolimnological records reveal how primary producers have responded to past environmental changes and thus provide insight on their future shifts. Sedimentary pigments are molecular biomarkers that can record detailed information about soft-bodied algae and cyanobacteria, which are not well represented by more conventional proxies. We analyzed diverse sedimentary pigments (echinenone, okenone, alloxanthin, canthaxanthin,  $\beta$ -carotene, and chlorophyll-*a* and its degradation products) from two cores using HPLC-MS, as well as bulk sediment organic and inorganic geochemistry, to reconstruct Holocene changes in primary production in a small, subarctic lake in South Greenland. We find multi-proxy evidence for a multi-millennial, mid-Holocene period of hypolimnetic anoxia from 6650 to 3500 cal yr BP within part of the lake. We suggest that summer thermal stratification and high productivity driven by warmer-than-present temperatures and increased catchment-derived nutrient influx drove changes in summer lakewater oxygenation. Our reconstructions reveal two distinct steady ecosystem states associated with oxygen status: a eukaryotic algae-dominated community during oxic conditions, versus cyanobacterial dominance during periods with anoxic bottom waters. Notably, we find that markers of anoxia and associated ecosystem shifts are stronger and probably longer-lived at one coring site, secondarily revealing considerable spatial (in addition to temporal) heterogeneity in oxygenation. As such, we propose that multi-core comparisons in paleolimnology can capture biogeochemical changes across both space and time, even in small lakes, and that spatial variations can provide clues about potentially localized drivers of past limnological change. Overall, our work broadly indicates that primary producer communities in some subarctic lakes were highly sensitive to warmer-than-present temperatures in the mid-Holocene, with landscape processes and thermal stratification playing secondary roles in driving productivity shifts. This implies that future warming could prompt widespread transformations in Arctic lake ecosystems, biogeochemistry (including carbon cycling and oxygenation), and water quality.

### 1. Introduction

The Arctic has been warming four times faster than the global average since the mid-20th century (Rantanen et al., 2022), and in response many Arctic regions are “greening”: melting ice and thawing permafrost have led to enhanced soil development, vegetation density, and aquatic primary production (Myers-Smith et al., 2020). Owing to dynamic glacial cycles, the Arctic landscape is characterized by an abundance of lakes, and their aquatic ecosystems are known to be more sensitive to climate-related changes than those at temperate latitudes or

high altitudes (Rühland et al., 2008; Schartau et al., 2022). Consequently, Arctic lake biota have been a major focus of research on climate-driven lacustrine ecosystem development, structure, and productivity, with associated implications for high-latitude carbon cycling as well as for Northern communities who rely on lakes for household water and other critical ecosystem services.

A paleolimnological approach provides for a robust understanding of productivity changes over a range of timescales, which is especially crucial in minimally instrumented Arctic regions. There are diverse views on what factors most strongly drive long-term changes in primary

\* Corresponding author. 2145 Sheridan Rd. – Tech F481, Evanston, IL, 60208, USA.

E-mail address: [miatuccillo@u.northwestern.edu](mailto:miatuccillo@u.northwestern.edu) (M.T. Tuccillo).

production within Arctic lakes (Fritz and Anderson, 2013): climate change is often considered the leading driver in high-latitude, terrestrial watersheds (Bouchard et al., 2017; Myers-Smith et al., 2020; Phoenix and Bjerke, 2016; Stevenson et al., 2021), but catchment processes, such as hydrological connectivity, runoff, or atmospheric delivery of nutrients, have been proposed as more influential in some regions (Massa et al., 2012; Prater et al., 2022; Wolfe et al., 2006).

Methodological limitations in paleolimnology may explain some of the uncertainties regarding drivers of Arctic lake productivity. In the Arctic, diatom species assemblages, cell counts, and siliceous structures quantified through sedimentary biogenic silica concentrations are the most common paleolimnological proxies for measuring aquatic biological responses to climate—e.g., with diatom abundance and assemblages being related to ice cover duration and, by extension, temperature (Smol, 1983). In Greenland (Kalaallit Nunaat), where our study focuses, stark climate-driven shifts in diatom abundances and assemblages are well-documented in lakes across the landmass (e.g., Perren et al., 2003, 2012; Saros et al., 2019). However, some studies reveal complex relationships between diatom ecology and temperature, with alternative drivers (e.g., land use, lake level, nutrient inputs, ice sheet/glacier proximity) primarily impacting diatom species assemblage shifts (e.g., Burpee et al., 2018; Massa et al., 2012; Prater et al., 2022). Moreover, metrics for bulk ecosystem productivity using singular classes of organisms offer incomplete generalizations of how the full diversity of primary producers respond to climate and other environmental changes (Catalan et al., 2013; Wolfe et al., 2006). This is especially true given that such changes may result in shifting ecosystem diversity (Schartau et al., 2022), where the disappearance of one class of primary producers (e.g., diatoms) may indicate rising dominance of another rather than simply a decrease in overall productivity.

Today, cyanobacteria are dominant contributors to phototrophic biomass in high-latitude lakes (Antoniades et al., 2009; Vincent and Quesada, 2012) in addition to being potentially detrimental to the quality of drinking water supplies in Greenland and beyond (Maréchal et al., 2023). However, they are often unaccounted for in paleolimnological studies due to their lack of siliceous or chitinous remains. To address this major gap in our picture of long-term changes in lake microbial ecosystems, this study employs a molecular biomarker approach—the quantification of numerous sedimentary photosynthetic pigments using High Performance Liquid Chromatography – Mass Spectrometry (HPLC-MS)—to evaluate the nature, timing, and drivers of shifts in a wider diversity of primary producers in a remote, upland lake near subarctic Narsarsuaq, Greenland.

Pigments in lake sediments are sourced from planktonic and benthic algae, cyanobacteria, aquatic or terrestrial higher plants, and macrophytes, and have key strengths as proxies: they have diverse chemical structures but derive from common biosynthetic pathways, and they are ubiquitous among phototrophic organisms but individually diagnostic of broader ecosystem members (Leavitt and Hodgson, 2002; McGowan, 2007). Furthermore, the presence of okenone, which derives from environmentally specialized anoxic purple sulfur bacteria, can highlight past periods of anoxia that are otherwise difficult to resolve (e.g., Fulton et al., 2018). Although the pigment chlorophyll-*a* and its derivatives have been widely measured and reported in lake sediments, so far there has been only limited quantification of individual carotenoid pigments in Arctic and Antarctic lakes, despite their demonstrated potential to illuminate microbial ecosystem change (Florian et al., 2015; McGowan et al., 2018; Reuss et al., 2013; Squier et al., 2002). For example, a 20-year, annually-varved sediment record in a Canadian lake recorded nutrient-driven eutrophication through a dramatic increase in cyanobacterial pigments, while diatom-associated pigments and more conventional eukaryotic algal biomarkers showed no change (Leavitt and Findlay, 1994).

In this study, we reconstruct Holocene primary producer ecosystems of a small upland lake in South Greenland. Lake Mel3 (informal name) is on a plateau removed from local anthropogenic influences but in a

region known to have experienced large insolation-driven climate shifts throughout the Holocene. We provide  $^{14}\text{C}$  chronologies for 2 sediment cores from Mel3 and track relative abundances of primary producers by quantifying sedimentary pigment biomarkers using HPLC-MS and comparing these measurements to sedimentary abundances of biogenic silica. Furthermore, we measure total sediment organic carbon (TOC), nitrogen (TN), and stable isotopes of organic C and N in bulk sediments. We also examine changes in bulk sediment elemental composition (by X-Ray Fluorescence) to infer landscape processes. Together, these proxies shed light on how a diverse ecosystem of primary producers responded to climatic and catchment processes over the Holocene.

## 2. Methods

### 2.1. Study design

#### 2.1.1. Regional and climatic settings

Lake Mel3 (N 61.12967, W 45.33630) is ~10 km southeast of Narsarsuaq, Greenland (Fig. 1a). The lake sits 849 m above sea level (a.s.l.) on the Mellemandet plateau between two outlet glaciers (Kiattut Sermiat and Qooqqup Sermia). Both glaciers have elevations lower than Mel3 today, with paleolimnological evidence pointing to Kiattut Sermiat's maximum Holocene elevation of 670 m a.s.l. during an unusual advance between ~4500–3000 cal yr BP (Pleuro and Axford, 2023). The uplands of the plateau have remained ice-free since regional deglaciation 11,100–10,500 cal yr BP (Carlson et al., 2014; Nelson et al., 2014; Pleuro and Axford, 2023) so glacier ice or meltwater have not influenced Mel3's waters for the duration of our Holocene lake sediment record.

The mean annual air temperature from 1981 to 2001 CE was 1.1 °C at the lower-elevation Narsarsuaq meteorological station (30 m a.s.l.), with mean winter and summer month temperatures of −7.3 and 10.8 °C, respectively. Warm summers are attributed to Narsarsuaq's continentality: Narsarsuaq sits within one of Greenland's very small zones of subarctic climate and vegetation, near sea level at the sheltered head of a fjord. However, Mel3's mean air temperatures are likely lower due to the study site's higher elevation. For instance, diurnal changes in air temperatures at Mel3 during field work in August 2022 were recorded to range from 1 to 6 °C, whereas Narsarsuaq meteorological station recorded contemporaneous highs and lows of 12.3 and 6.5 °C respectively (Danish Meteorological Institute). There is only very thin, highly discontinuous soil cover in the lake's watershed on the bedrock plateau, with sparse vegetation cover consisting of patchy dwarf shrubs, forbs, grasses and sedges (Fig. 1b).

#### 2.1.2. Study site

Lake Mel3 (0.1 km<sup>2</sup>, maximum depth of 13.1 m) is hydrologically through-flowing in typical conditions today, although satellite imagery suggests it may rarely become a closed basin in some years. Mel3 receives its water from snowmelt, precipitation, and precipitation runoff over a 0.5 km<sup>2</sup> watershed that includes a smaller upstream lake northeast and ultimately drains via surface outflow southwest off the plateau into the surrounding fjord (Fig. 1). The stream connection from the upstream lake is ~370 m long, and field observations indicate that discharge fluctuates strongly through the spring and summer, presumably in response to snowmelt intensity. The upstream lake may become hydrologically disconnected when snowmelt inputs decline and upstream lake level drops.

Mel3's lake bottom is covered with soft sediments between boulders, with patchy benthic aquatic mosses. Nearest to the inlet stream is Mel3's steepest wall, immediately east of the lake's depocenter and our deepest coring site (site A at 13.1 m depth), situated only 50 m from the modern-day shoreline. The second-deepest coring site (at 12.1 m depth, site B) is located ~60 m southwest and towards the lake's center; the two sites are separated by a small bathymetric rise within the depocenter (Fig. 1c). Secchi disk visibility in August 2022 reached to the lake's maximum depth (13.1m), indicative of ultra-oligotrophic waters. Plankton tows

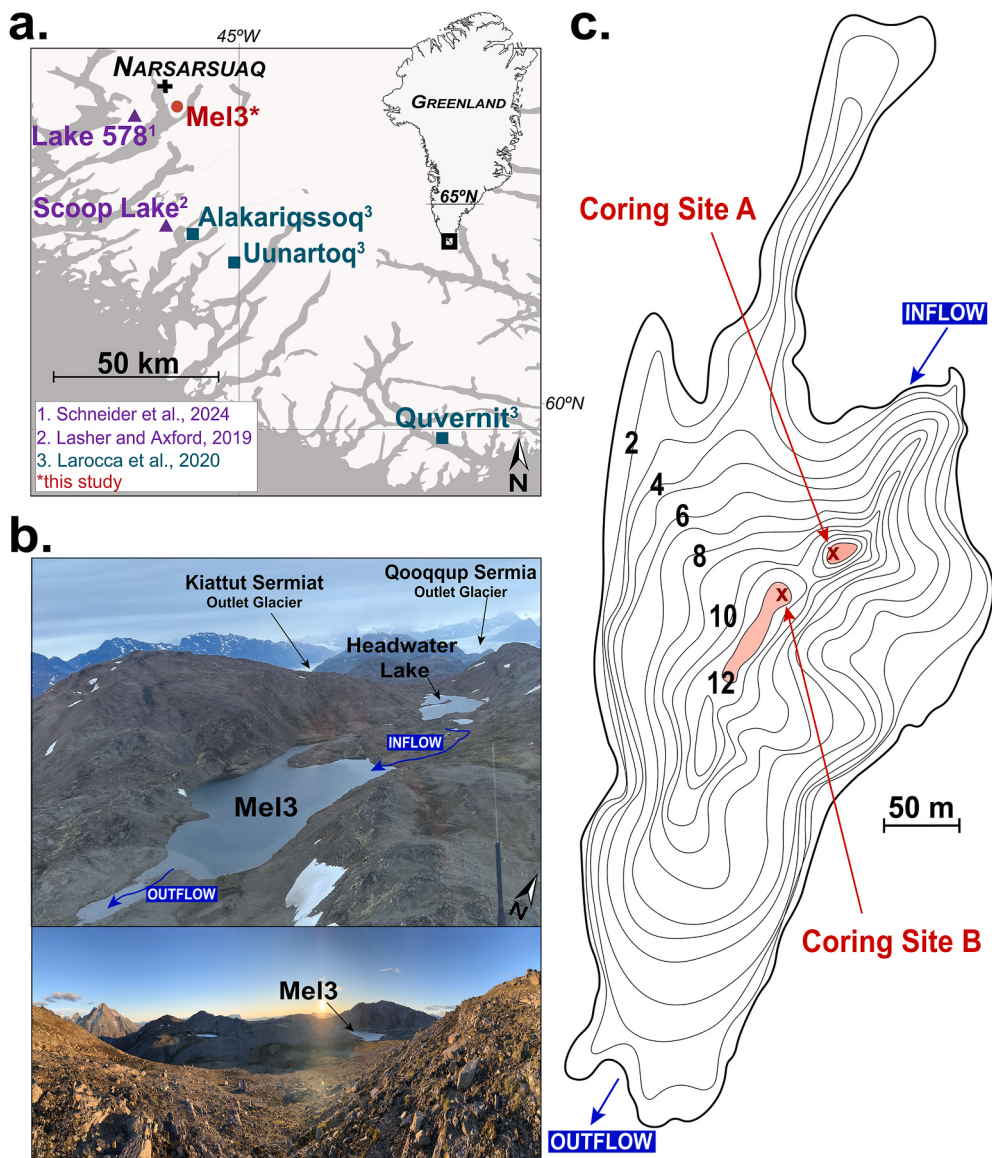


**Fig. 1. Geographical context, bathymetry and catchment photos of Lake Mel3.** (a) Study region in subarctic South Greenland with relevant sites including Mel3 (red circle), the town of Narsarsuaq (black cross), and local limnological records (purple triangles) and mountain glaciers (blue squares) referenced in the text (see Fig. 5). Grey = water, white = land/ice; (b) Field photos of Lake Mel3's bedrock, bouldery catchment with limited vegetation cover and minimal soil development, including Mel3's headwater lake, surface inflow and outflow streams, and local, lower-elevation outlet glaciers of the Greenland Ice Sheet; (c) Mel3's bathymetry, with local bathymetric lows around coring sites A and B shaded in red (contours represent 1 m) and coring sites marked with red X's. (For interpretation of the references to color in this figure legend, the reader is referred to the Web version of this article.)

demonstrated a zooplankton-rich aquatic community, with copepods dominating.

#### 2.1.3. Field methods and sample handling

On August 5–7 of 2022, one long sediment core (1.84 m) and a shorter surface core (56 cm) were collected from Mel3 using a Nesje percussion piston system and an Aquatic Research Instruments “Universal” check-valve percussion coring system, respectively. The longer piston core (core N1) was retrieved from Mel3’s deepest point (coring site A) while the surface core (core U3) was collected 60 m to the west (coring site B). Core U3 had a well-preserved sediment-water interface and was collected in a clear polycarbonate tube that was promptly wrapped in duct tape to prevent light penetration and maximize pigment preservation. N1 was collected in an opaque PVC tube and cut in the field into two lengths for transport. All cores were transferred to Northwestern University intact and stored at 4 °C until analysis.

Core U3 was split at Northwestern University in September 2022 and

sectioned into 1 cm intervals under low light to prevent pigment photodegradation. N1 was split in October 2022 and sub-sampled under low light with varying resolution: the core showed considerable color changes, including sections of dominantly black or brown laminated sediments (sampled in 2 cm increments), sediments with intermediate or fluctuating color (sampled in 1 cm increments), and individual isolated color bands (1–2 cm, sectioned separately depending on thickness). Immediately after sectioning, sediment aliquots were flushed with N<sub>2</sub> and frozen in glass amber vials at –20 °C until pigment, biogenic silica, and organic geochemical analyses.

#### 2.2. Laboratory methods and data analysis

##### 2.2.1. Chronology

Terrestrial and aquatic macrofossils were extracted from sediments in all cores, cleaned with ultra-pure water, and sent to the Woods Hole Oceanographic Institute National Ocean Sciences Accelerator Mass

Spectrometry facility (WHOI-NOSAMS) for AMS  $^{14}\text{C}$  analysis. To assess the viability of dating aquatic materials at this site, we dated paired terrestrial and aquatic macrofossils at several depths in core U3 and found a consistent radiocarbon offset of  $\sim 600$  years between older aquatic moss and younger terrestrial macrofossils (leaf/wood) (Fig. 2b). This likely reflects leaching from small amounts of metasedimentary carbonate-bearing glacial drift from Mellamlandet's bedrock, which includes the Gardar Province ( $\sim 1300$ – $1140$  Ma syenite, gabbro and carbonatite; Upton et al., 2003; Puleo and Axford, 2023), into the lakewaters of Mel3. Consequently, only terrestrial macrofossil radiocarbon ages were used to construct age models. Terrestrial macrofossils consisted of twigs and leaves mostly identified as *Betula* spp. and were found in adequate abundance for dating except for in the top 5 cm of U3 and base of N1. CALIB version 8.2 (Stuiver et al., 2022) was used to calibrate individual radiocarbon ages, and the R package rBacon was used to create a Bayesian age-depth models for both cores using the IntCal20 calibration curve (Reimer et al., 2020).

Sedimentation rate (cm/year) was calculated between each discrete radiocarbon age (e.g., cm between each sampled macrofossil/years between each median calibrated age). Dry mass accumulation rates ( $\text{g year}^{-1} \text{cm}^{-2}$ ) were calculated through multiplying sedimentation rate by dry bulk density ( $\text{g cm}^{-3}$ ), which was measured through volume-controlled sampling of wet sediments prior to lyophilization.

### 2.2.2. Bulk organic and inorganic parameters

Freeze-dried sediments from a few representative depths were examined for the presence of carbonate minerals using diffuse reflectance Infrared Fourier Transform Spectroscopy (DRIFTS) (So et al., 2020). As no carbonate peaks were present for any samples (likely absence through in-situ weathering or leaching/biological uptake of any very small carbonate inputs prior to sedimentation), sediments were not

acidified prior to  $\delta^{13}\text{C}$  and TOC analyses. Dry sediments from cores N1 and U3 and any macrofossils within were ground until homogenous using a methanol-rinsed ceramic mortar and pestle and analyzed for % wt. OC, % wt. N,  $\delta^{15}\text{N}$  and  $\delta^{13}\text{C}$  using a Costech 4010 Elemental Analyzer and Themo Scientific Delta V Plus Isotope Ratio Mass Spectrometer (EA-IRMS; Northwestern University Stable Isotope Laboratory). Samples were run alongside replicate certified lab standards (Acetanilide #1 and Urea #2; Arndt Schimmelmann, Dept. of Geological Sciences, Indiana University) and corrected for linearity and instrument drift.

Isotopic measurements here are expressed in the  $\delta^{15}\text{N}$  and  $\delta^{13}\text{C}$  notations (relative to air and the Vienna PeeDee Belemnite (VPDB) reference standard, respectively). Analytical uncertainty is  $< 0.3\text{‰}$  for both  $\delta^{15}\text{N}$  and  $\delta^{13}\text{C}$  measurements.  $\delta^{15}\text{N}$  values of bulk sediment, which include both the organic N fraction within organic compounds as well as inorganic forms, are commonly used in Greenland lake sediments to understand the origin and magnitude of nitrogen influx and availability for primary productivity (e.g., Hobbs et al., 2010; Wolfe et al., 2006).  $\delta^{13}\text{C}$  values of bulk sediment reflect different sources of organic matter, with lower values in Arctic lakes typically being attributed to lacustrine algae and higher values ascribed to C4 terrestrial plants (Hobbs et al., 2010; Wolfe et al., 2006). Finally, C/N ratios were calculated to estimate the relative contributions of cellulose-rich terrestrial organic matter to protein-rich aquatic organic matter (e.g., higher C/N ratios indicate higher terrestrial input).

Each sediment interval was analyzed for % wt. biogenic silica to estimate bulk abundance of diatoms following Mortlock and Froelich (1989). Briefly, sediment was digested in HCl and  $\text{H}_2\text{O}_2$  to remove organic matter and then extracted in 10 % sodium carbonate solution before reduction by metol-sulfite and spectrophotometric analysis (single-peak absorbance, 812 nm). Final biogenic silica concentrations (mM) were calculated with a 10-point calibration curve from an

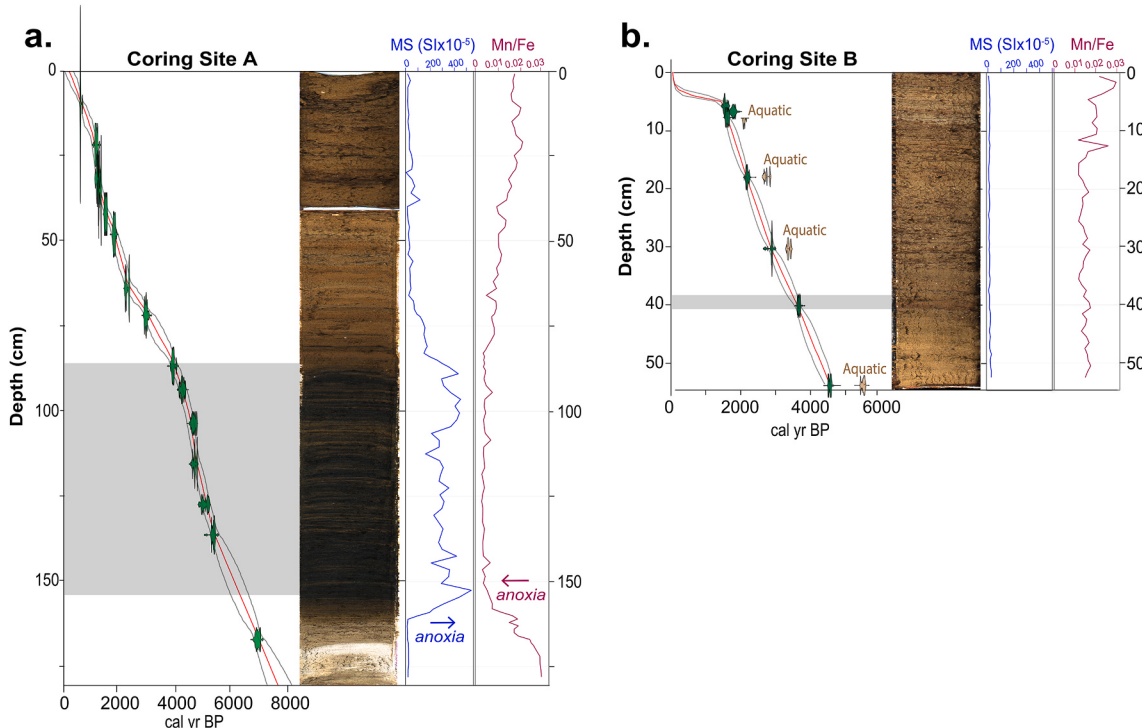


**Fig. 2. Radiocarbon age models, core images, and inorganic anoxia proxies in (a) core N1 and (b) core U3.** Green distributions indicate the 2-sigma calibration probability distribution for each terrestrial macrofossil age, red lines show best-fit mean Bayesian age model, and grey dotted lines show 95 % confidence intervals. Brown distributions in (b) indicate ages of aquatic moss macrofossils, which demonstrate a 600-year offset and are therefore not factored into the age model. Each core age model is accompanied by proxies for anoxic sedimentation, including magnetic susceptibility (MS; blue lines) and Mn/Fe ratios (purple lines) as measured by scanning XRF (Mewafy et al., 2011; Olsen et al., 2012). Grey shaded regions reflect depths associated with black sedimentary units evidencing anoxia in (a) and a potential period of hypoxia in (b). The horizontal white band at 34 cm depth in the image of core N1 is a gap where the core was chopped into two sections in the field. (For interpretation of the references to color in this figure legend, the reader is referred to the Web version of this article.)

ultra-pure analytical standard and subsequently normalized to dry mass per sample for dry weight percent (wt. % biogenic silica). While multiple sources can contribute to biogenic silica fraction (e.g., sponge spicules, chrysophytes), smear slides from Mel3 revealed only diatom valves and prior paleolimnological work in Greenland interprets diatom production as the major contributor to sedimentary biogenic silica, which is thus proposed as a suitable proxy for diatom abundance (Kaplan et al., 2002; Reuss et al., 2013).

Freshly split cores were scanned on a GeoTek-MSCL-S core scanner, equipped with an Olympus DELTA Professional X-Ray Fluorescence (XRF) spectral detector and a Bartington MS2E magnetic susceptibility sensor, to yield estimated elemental abundances in bulk sediments (e.g., Ti as a proxy for landscape runoff; Makri et al., 2019), magnetic susceptibility, and high-resolution core images.

Given the absence of carbonates in Mel3's sediments (DRIFTS analysis, see above), we could calculate fluxes of Mel3's primary sedimentary components by weight: biogenic silica wt. %, total organic matter (TOM) wt. %, and minerogenic material wt. %. By convention, TOM was estimated by multiplying TOC by a conversion factor of 1.724 (Pribyl, 2010). The minerogenic component was calculated as the sedimentary contribution that was not biogenic silica or TOM (i.e., out of 100 %) for each sediment interval. Fluxes were calculated following Prater et al. (2022); given that measured and calculated wt. % are normalized to dry sediment, we multiplied component wt. % by sedimentary dry mass accumulation rate to estimate component flux. Fluxes provide additional insight on whether changes in raw measurements are driven by true increases/decreases or concurrent changes in sedimentation.

### 2.2.3. Pigments

Sedimentary pigments were quantified in this study with a mass-based approach. Although spectrophotometric analysis is common (e.g., many pigments have overlapping absorbances that make them indistinguishable), and because their light absorption is tied to excitation of electrons in conjugated double bond structures, their diagenetically-saturated derivatives contribute to uncertainties in spectrophotometric identification (McGowan, 2007). To resolve more pigment types and their derivatives than can be accomplished with spectrophotometric analyses, our approach uses HPLC combined with ultra high-resolution mass spectrometry (MS) to quantify a broader suite of pigments with diagnostic resolution for different ecosystem members (Airs et al., 2001; Squier et al., 2002).

To extract pigments, 5 mL of HPLC-grade acetone (100 %) was added to known masses of dry lake sediment immediately after lyophilization. Extracts were shaken vigorously and then sonicated for 10 min in an ultrasonic bath to break apart cells. Vials were flushed with N<sub>2</sub> and then incubated at -20 °C for 24 h (Florian et al., 2015). Extracts were then centrifuged at 4200 rpm for 10 min, and the supernatant was filtered through 0.2 µm PTFE syringe filters. The final extracts were dried under N<sub>2</sub> and stored at -20 °C; Airs et al. (2001) found these conditions sufficient to ensure pigment stability for up to 2 years until analysis. Immediately before injection, extracts were re-suspended in 1 mL ultra-pure HPLC-grade ethanol (>99.5 %). Samples were vortexed for dissolution before being transferred to amber autosampler vials and injected into an Agilent UHPLC-QTOF-MS (Ultra-HPLC-Quadrupole time-of-flight-MS) at Northwestern University's IMSERC facility (Integrated Molecular Structure Education and Research Center). The instrument was equipped with a C18 column (150 mm) to maintain maximum hydrophobicity, and two mobile phases: (A) 9:1 Water: Methanol solution, and (B) 2:3:5 Acetonitrile:Methanol:Isopropyl Alcohol. Samples were injected at a flow rate of 0.2 mL/min for 13 min (solvent schedule: Table S1). Elution times for our pigment compounds ranged from 4 to 9 min.

Seven sedimentary pigments and one sterol chlorin ester (SCE) were analyzed— six of which were quantified using external reference standards (canthaxanthin, alloxanthin, echinenone, β-carotene, chlorophyll-a and pheophytin-α; DHI Denmark). Calibration curves of DHI reference

standards of known concentrations were constructed using 3- to 6-point serial dilutions;  $r^2$  values ranged from 0.96 to 1.00 (Fig. S1). Well-resolved retention times (Table S2) and a "Find-By-Formula" targeted approach in Agilent MassHunter™ Qualitative Analysis software was used to identify pigments. Peak areas were used to calculate concentrations from external standard calibration curves before being normalized to dry sediment weight and ultimately normalized to TOC (ng<sub>pigment</sub> g<sub>OC</sub><sup>-1</sup>).

Pigments without commercial standards (okenone and the SCE pyropheophorbide-α) were extracted from modern day samples and run in triplicate on the HPLC-QTOF-MS to constrain retention times. Okenone, which derives from anoxic photosynthetic bacteria (purple S bacteria) and is known to be preserved in lake sediments (Fulton et al., 2018), was measured through comparison to a purple S bacterial culture at Northwestern University. Pyropheophorbide-α (a SCE of Chlorophyll-a produced exclusively in the intestinal tract of grazing zooplankton; Harradine et al., 1996; Itoh et al., 2007) was measured through comparison to a frozen sample from a modern-day plankton tow sampled from lake Mel3 in August 2022 and containing abundant copepods. The concentrations of okenone and pyropheophorbide-α in sediments for this study are reported as relative abundances downcore (e.g., peak areas normalized to the highest peak area detected across the basin).

## 3. Results

### 3.1. Chronology and stratigraphy

**Coring site A:** Calibrated ages for 15 terrestrial macrofossils in piston core N1 span nearly 8000 years. Age control on the basal 30 cm of sediment is weak given lack of aquatic or terrestrial macrofossils suitable for dating (Fig. 2a). Ages follow sequential continuity with depths throughout the transition, and sedimentation rates remain relatively steady despite major stratigraphic transitions.

The basal sediments are grey, dense lake sediments devoid of aquatic moss remains or other organic remains but containing abundant diatoms in smear slides. The bottom-most radiocarbon date (~7053 cal yr BP) marks the onset of dark brown gyttja deposition, with visible laminations and abundant aquatic mosses. Between 6650 and 3500 cal yr BP, the N1 core preserves black, laminated sediments (Fig. 2a) which visibly oxidized (to reddish) after the core was split. Such reduced layers also contain elevated magnetic susceptibility values and decreased Mn/Fe ratios (Fig. 2a), which along with the sediments' black color indicate anoxic deposition (Olsen et al., 2012; Mewafy et al., 2011). The remainder of the core is brown gyttja, with a coarser dense unit beginning ~2900 cal yr BP and transitioning over 1000 cal yr to mossy, organic-rich sediments that extend to the top of the core.

**Coring site B:** Paired terrestrial and aquatic macrofossils dated at four depths in core U3 demonstrate a significant radiocarbon offset, with aquatic mosses dating ~600 cal yr older likely due to a hardwater effect of leaching from minor amounts of carbonate-bearing glacial drift into Mel3's dissolved carbon pool (Fig. 2b). Therefore, our age model is based exclusively on terrestrial macrofossils' ages, which show a steady sedimentation rate between bottom-most and top-most dates (4479 cal yr BP to 1398 cal yr BP). Dateable macrofossils are absent above 5 cm, so our chronological model terminates in the late-Holocene, where there is also a notable implied change in sedimentation rate or perhaps sediments missing from this core recovered with an open check-valve (piston-less) system. For the purposes of this study examining multi-millennial ecosystem changes through the Holocene, we focus on core zones with strong geochronology and demonstrably intact, continuous sedimentation: coring site B's record from ~4400 to 1500 cal yr BP and coring site A's > 7000-yr record. Sedimentation rates during the period of focus where cores overlap are nearly the same (0.014 cm/year for U3 and very slightly faster at 0.017 cm/year for N1 for 4400–1500 cal yr BP) despite differences between the coring sites and coring devices used.

Coarse and minerogenic basal sediments in core U3 contain a low abundance of aquatic moss macrofossils and bear little resemblance to the temporally equivalent black, laminated unit in core N1 except for a small 2–3 cm band of black and brown sediments that terminates at ~3800 cal yr BP (Fig. 2b), potentially indicating a short period of reducing conditions. Laminated sediments throughout the mid-to late-Holocene transition (~3500–1500 cal yr BP) are organic and rich in aquatic mosses.

### 3.2. Organic geochemical proxies

**Coring site A:** Basal sediments in core N1 preserve the lowest TOC and TN of the record (~1.25 wt % and ~0 wt %, respectively; Fig. 3a–c). The basal unit is followed by abrupt rises in TOC and TN (by ~5 wt % and 0.5 wt %, respectively) at ~7500 cal yr BP. Though the onset of black, reduced sediments ~6650 cal yr BP is accompanied with slight declines in TOC and TN (by ~1 and ~0.1 wt %, respectively), TOC and TN remained high throughout the inferred anoxic unit and into the late-Holocene, ranging from 3 to 7 wt % and 0.3–0.5 wt %, respectively.

We ascribe extremely high and unrealistic C/N ratios in the basal sediments of core N1 to near-zero (<0.05 %) TN values. However, high  $\delta^{13}\text{C}$  values (up to ~−15 ‰) in these sediments still indicate terrestrial sources of organic matter (Meyers, 1994). Sediments became gradually more  $^{13}\text{C}$ -depleted into the subsequent period of inferred anoxia (Fig. 3b).  $\delta^{15}\text{N}$  values experienced large shifts, rising by almost 2 % at 7500 cal yr BP and then declining by 2 % between 7100 and 6650 cal yr BP leading up to the onset of anoxia (Fig. 3d). Sedimentary  $\delta^{15}\text{N}$  values remained low (−1 to 0 ‰) throughout the inferred anoxic period from 6650 to 3500 cal yr BP. At 3500 cal yr BP,  $\delta^{15}\text{N}$  and  $\delta^{13}\text{C}$  values increased, marking a period of  $^{15}\text{N}$ -enrichment (increase in  $\delta^{15}\text{N}$  value by ~0.5 ‰ compared to the anoxic period). Sediments became both increasingly  $^{15}\text{N}$ -enriched (reaching peak  $\delta^{15}\text{N}$  values of +1.5 ‰) and  $^{13}\text{C}$ -depleted (reaching record-low values of  $\delta^{13}\text{C} = -27$  ‰) from 2000 to 1000 cal yr BP alongside a positive shift in C/N ratios, indicating increasing productivity and contributions of allochthonous organic matter (Fig. 3e). A sharp decrease in C/N ratios occurred at ~1000 cal yr BP; C/N ratios remain low until present. Sub-basin A sediments

demonstrate a mixed source of organic matter, with  $\delta^{13}\text{C}$  and C/N values falling between aquatic and terrestrial endmembers (Meyers, 1994).

**Coring site B:** TOC and TN concentrations ranged from lowest values at the beginning of record (~1.5 wt %) to nearly an order of magnitude higher in recent sediments (~10 wt %; Fig. 3a–c). Substantial increases in TOC (by ~5 wt %) and TN (by ~0.6 wt %) occurred at ~3500 cal yr BP and stabilized before decreasing in the late Holocene (by 2 wt % at ~1500 cal yr BP).

Compared to coring site A,  $\delta^{15}\text{N}$  and  $\delta^{13}\text{C}$  values in coring site B remained mostly stable throughout the whole record (Fig. 3b–d). Sediments are slightly  $^{15}\text{N}$ -depleted and  $^{13}\text{C}$ -depleted in the period of potential hypoxia from 4400 until 3800 cal yr BP, where  $\delta^{15}\text{N}$  and  $\delta^{13}\text{C}$  values increase gradually until the late-Holocene (by 0.5 ‰ and 2 ‰, respectively). Notably, sediments from the shallower and more central coring site B both have enriched  $\delta^{13}\text{C}$  and  $\delta^{15}\text{N}$  values compared to core N1 (coring site A, which is closer to the lake's main inflow) throughout the Holocene (+3 ‰ and +1.5 ‰ more enriched, respectively).

### 3.3. Pigments and productivity

**Coring site A:** In the basal sediments >7500 cal yr BP, all pigments except for pheophytin- $\alpha$  and pyropheophorbide- $\alpha$  (degradation products of chlorophyll- $\alpha$  associated with diagenesis and zooplankton grazing respectively) were at or below detection limits (Fig. 4). The high relative pheophytin- $\alpha$  concentration during chlorophyll- $\alpha$ 's absence probably indicates poor overall pigment preservation early in the record (Fig. 4c; Reuss et al., 2013). The biogenic silica pulse recorded at ~7500 cal yr BP (reaching 40 wt %) occurred while pyropheophorbide- $\alpha$  decreased below detection limit. All pigment concentrations increased ~500 years after the biogenic silica peak, followed by concentrations of chlorophyll- $\alpha$ ,  $\beta$ -carotene, and alloxanthin dropping below detection limit at the onset of inferred anoxia at 6650 cal yr BP. Biogenic silica also gradually decreased into the anoxic period, both as a percentage and a flux (Fig. 4a; Fig. 5e).

The period of anoxia is distinctly characterized by the highest relative abundance of okenone, a key biomarker for anoxia in lakes (Fulton et al., 2018). Echinone and canthaxanthin, produced by

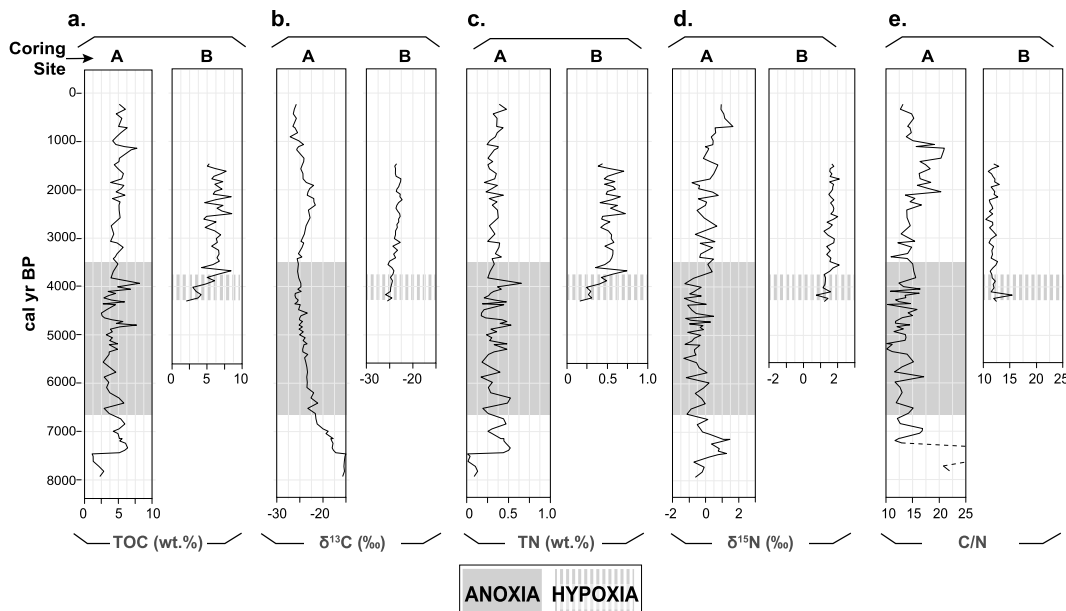


**Fig. 3. Organic geochemical proxies for source and amount of organic matter in bulk sediments in cores from coring sites A and B.** (a) Total organic carbon (TOC) as percent of dry sediment weight; (b)  $\delta^{13}\text{C}$  (‰) relative to the Vienna PeeDee Belemnite (VPDB); (c) total nitrogen (TN) as percent of dry sediment weight; (d)  $\delta^{15}\text{N}$  (‰) relative to air; (e) TOC/TN ratio, with dashed lines in the earliest part of core N1's record indicating that values may be unreliable due to near-zero (<0.05 ‰) TN abundances. Grey shaded zones are inferred periods of anoxia for coring site A, and dashed grey zones indicate a potential period of hypoxia for coring site B based upon stratigraphic observations and okenone concentrations.

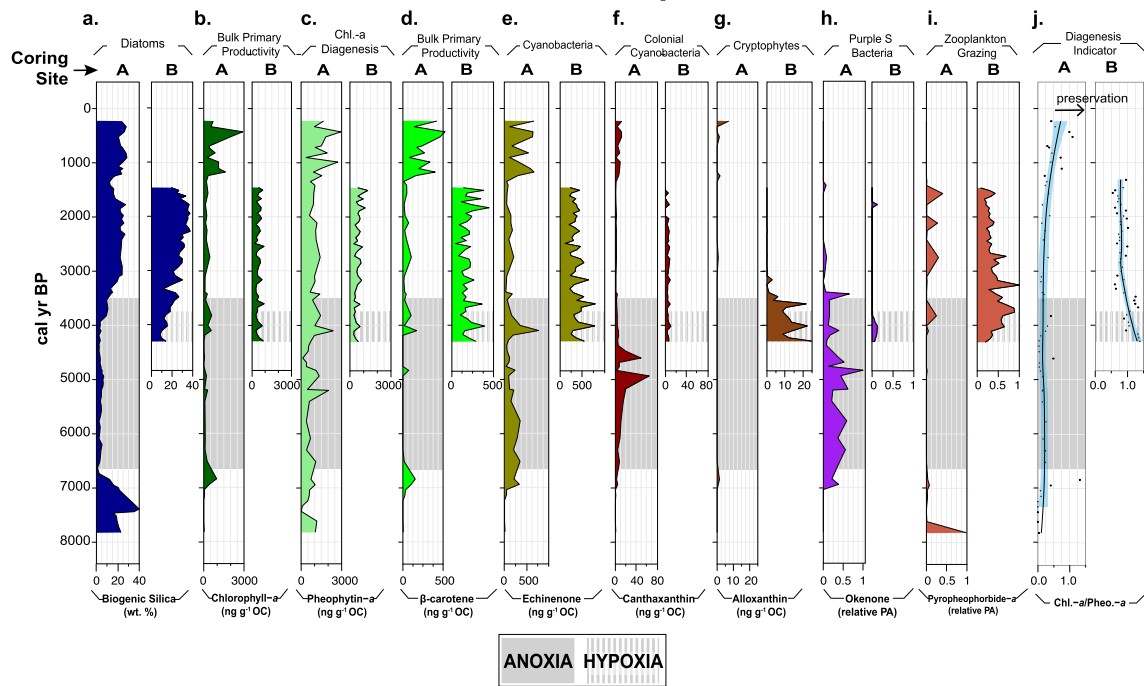


**Fig. 4. Primary productivity proxies throughout the mid-to-late Holocene for coring sites A and B.** (a) Diatom production, measured through sedimentary biogenic silica as weight percent of dry sediment; (b–j) pigments indicative of bulk productivity and/or algal and cyanobacterial species. (b–g) are quantified using external reference standards and normalized to dry sediment weight and ultimately g OC; (h–i) are reported as peak area relative to standards created in our lab (see Methods). Ratios between chlorophyll-*a* and pheophytin-*a* in (j) indicate preservation index; black line indicates mean (LOESS smoothing) between data points, and blue distributions display 95 % confidence intervals. Grey shading across all panels indicates periods of anoxia for coring site A, and dashed grey zones indicate a potential period of hypoxia for coring site B as described in the text. (For interpretation of the references to color in this figure legend, the reader is referred to the Web version of this article.)

cyanobacteria and more specifically colonial and blooming cyanobacteria respectively, remained stable or increased in anoxic conditions (Fig. 4e and f). Canthaxanthin distinctly peaked in the middle of this period (~5000 cal yr BP). Biogenic silica and pigments indicative of bulk algal primary productivity (e.g., chlorophyll-*a* and  $\beta$ -carotene) and zooplankton predation (pyropheophorbide-*a*) reached lowest record values in the core. While still detected, pheophytin-*a* concentrations were among the lowest of the record during the period of anoxia.

Increases in biogenic silica, chlorophyll-*a*,  $\beta$ -carotene, and pyropheophorbide-*a* occurred at the end of the anoxic period (3500 cal yr BP). Meanwhile, cyanobacterial pigments (echinenone, canthaxanthin, and okenone) decreased and remained low until 1200 cal yr BP. In the late-Holocene, a sudden increase in all primary productivity pigments except for okenone and alloxanthin occurred at ~1200 cal yr BP, with concentrations of echinenone,  $\beta$ -carotene, chlorophyll-*a* and pheophytin-*a* each almost tripling. These uniquely high values relative to the rest of the core also correspond with an increase in chlorophyll-*a* to pheophytin-*a* ratio, which indicates that preservation is highest in the late-Holocene during this period. However, it is likely that preservation alone is not solely responsible but may amplify a true increase in all primary producer biomarkers, as this trend parallels an increase in biogenic silica to the second-highest concentrations throughout the record. Pyropheophorbide-*a*, on the other hand, remained below detection limit, implying decreased zooplankton grazing. These concentrations of pigments and biogenic silica in the late Holocene remained stable to present.

**Coring site B:** The U3 sedimentary pigment record includes several dominant transitions where green algal/plant pigments parallel biogenic silica trends, and other carotenoids fluctuate independently. Though alloxanthin (derived from cryptophytes) is low in all Mel3 sediments (<20 ng/g OC), the period from the base of the core ~4400 to 3500 cal yr BP has peak alloxanthin concentrations. Low (scaled to the

highest peak area detected in core N1) but detectable okenone abundance from 4400 to 3800 cal yr BP indicates a potential period of hypoxia (reduced oxygen conditions), during which concentrations of chlorophyll-*a*, pheophytin-*a*,  $\beta$ -carotene and cyanobacterial pigments (echinenone, canthaxanthin) remain stable (Fig. 4). Finally, sedimentary concentrations of  $\beta$ -carotene increased around 2000 cal yr BP and reached their peaks alongside biogenic silica while pyropheophorbide-*a* decreased to record lows, indicating reduced grazing.

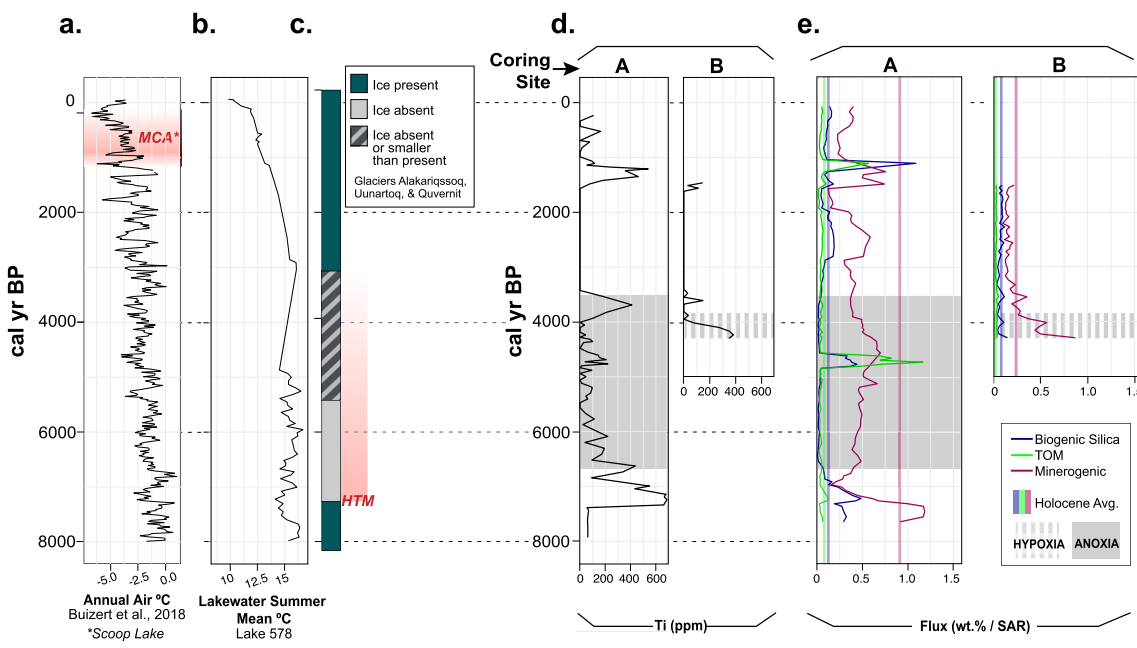
Coring site B's pigment record deviates from coring site A in three main ways: First, sediments preserve very low okenone concentrations at site B for the duration of inferred anoxia in coring site A, with detectable sedimentary okenone only present from the base of the record to 3800 cal yr BP in coring site B. Secondly, coring site B's sediments show high alloxanthin values (from cryptophytes) 4400–3500 cal yr BP while coring site A sediments preserve little detectable alloxanthin. Finally, all other sedimentary pigment concentrations except for okenone in coring site B's sediments are consistently higher than for coring site A.

## 4. Discussion

### 4.1. Evidence for and effects of oxygenation changes on primary productivity

#### 4.1.1. Evidence for anoxia

Although only one site (coring site A) showed prolonged, multi-proxy sedimentological evidence for anoxia (Fig. 2), both coring sites preserve evidence for reduced oxygen in the mid-Holocene. The presence of the pigment okenone in coring site A's sediments from 6650 to 3500 cal yr BP—in contrast with its absence or low values in the remainder of the Mel3 sequence—records the prominence of purple S bacteria, indicating an anoxic photic zone for almost three thousand



### REGIONAL TEMPERATURE RECORDS

### MEL3: FLUXES AND LANDSCAPE MINERAL PROXIES

**Fig. 5. Periods of anoxia and hypoxia at Mel3 compared with regional climate records and proxies for major sediment components.** (a) Annual air temperature at Narsarsuaq ( $^{\circ}\text{C}$ ), ice core-based and modeled reconstruction; Buizert et al., 2018). Red zone indicates the Medieval Climate Anomaly (MCA) as reconstructed by Lasher and Axford (2019) at Scoop Lake (see Fig. 1a); (b) Summer mean water temperature (SMWT,  $^{\circ}\text{C}$ ; biomarker-based reconstruction) at Lake 578 (see Fig. 1a; Schneider et al., 2024); (c) regional mountain glacier response to warming (limnological and geospatial analyses, see Fig. 1a; Larocca et al., 2020); red shaded zone reflects the timing of the Holocene Thermal Maximum inferred from this local glacier record. Mel3 proxies for terrigenous input include (d) Ti concentrations (black lines) and (e) fluxes of mineral material (purple), which are also plotted against fluxes of major sedimentary components biogenic silica (blue) and TOM (total organic matter; green). Fluxes are presented as dry mass accumulation rates (see Methods). Holocene mean fluxes are shown as vertical lines. Grey zones (d–e) show period of anoxia at coring site A and grey dashed zones show potential hypoxia at coring site B. SAR = sediment accumulation rate. (For interpretation of the references to color in this figure legend, the reader is referred to the Web version of this article.)

years during the middle Holocene at the deepest core site (Fig. 4h; Dreßler et al., 2007; Fulton et al., 2018). Additionally, the concomitant decrease in Mn/Fe ratio for core N1 between 6650 and 3500 cal yr BP reflects Mn's enhanced solubility compared to Fe under reducing conditions, and thus hypolimnetic anoxia (Fig. 2a; Davison, 1993; Olsen et al., 2012). Higher magnetic susceptibility in Unit IV also points to reducing conditions where more Fe is sedimented (e.g., Mewafy et al., 2011) (Fig. 2a).

While substantially less abundant than in coring site A, okenone is also preserved in sediments from coring site B starting at the base of the core (~4400 cal yr BP) and persisting until 3800 cal yr BP. The highest okenone values co-occur with a thin band of black and dark brown sediments that are unique in core U3, near the top of the okenone-bearing section. Despite this evidence for low-oxygen conditions, Mn/Fe and magnetic susceptibility values do not indicate anoxia at these depths. We interpret this more limited evidence for low-oxygen conditions as indicating potential hypoxia, rather than full anoxia, at site B. Together, these independent organic and inorganic proxies indicate that anoxia persisted from 6650 to 3500 cal yr BP at one site (core site A) and reduced oxygen conditions may have extended to both coring sites for a period of unknown duration ending at 3800 cal yr BP.

#### 4.1.2. High primary productivity prior to anoxia

The period prior to anoxia at coring site A is only recorded in the piston core (N1) from the deeper site. Lake sediments from this part of the early Holocene are defined by high biogenic silica concentrations (up to 40 wt % at ~7500 cal yr BP; note that ages for this sedimentary unit, below the deepest  $^{14}\text{C}$  age, are poorly constrained), even in the core's basal sediments (e.g., 25 wt % biogenic silica alongside 2.5 wt % TOC). This indicates that diatoms (which dominated smear slides, whereas chrysophytes were absent) were very abundant and were

Mel3's dominant primary producers in the early Holocene. Most primary producer pigment concentrations at this time (except for pheophytin-a, a degradation product of chlorophyll-a, which is produced by diatoms; Jeffrey and Veske, 1997) remained below detection until biogenic silica concentrations began to decrease at ~7400 cal yr BP. We ascribe the increase in concentrations and diversity of pigments indicative of bulk primary productivity (e.g.,  $\beta$ -carotene, chlorophyll-a) and cyanobacterial pigments (e.g., canthaxanthin, echinenone) to a diversifying ecosystem, as Holocene primary producer communities in Greenland lakes are known to demonstrate increasing species richness with lake ontogenetic age (Jeppesen et al., 2023). Regional summer temperatures were also increasing into the Holocene Thermal Maximum in South Greenland (Fréchette and de Vernal, 2009; Larocca et al., 2020; Schneider et al., 2024) at the time pigment assemblages were diversifying, suggesting that warmth may have additionally driven species diversity.

Very high diatom primary productivity directly preceded the period of mid-Holocene anoxia in lake Mel3. Much evidence elsewhere has linked high primary productivity, which accelerates carbon burial and respiration, with oxygen depletion in lakes in the Arctic and beyond (e.g., Deshpande et al., 2017). Furthermore, high primary productivity is known to impact lakewater turbidity and, in turn, radiative effects that indirectly provide conditions necessary for anoxia (e.g., Kirillin et al., 2012; McFarlin et al., 2023; Saros et al., 2016). We elaborate more on the causes of high productivity and the onset of anoxia in section 4.2.

#### 4.1.3. Aquatic ecosystem changes during anoxia

During Mel3's mid-Holocene low-oxygen period from 6650 to 3500 cal yr BP, we find evidence for low primary productivity of eukaryotic algae, including diatoms, and rule out low preservation or enhanced zooplankton grazing as potential causes. Although anoxic water

columns are generally associated with higher pigment preservation and sedimentary abundances (e.g., Woulds and Cowie, 2009), the period of inferred anoxic deposition in core N1 contains some of the lowest measured abundances of chlorophyll-*a*, pheophytin-*a*,  $\beta$ -carotene and alloxanthin of the record. This period is also characterized by the lowest concentrations of biogenic silica, which is not subject to the same oxygen-mediated diagenetic processes, supporting a reduction in diatom production. Moreover, ratios of chlorophyll-*a* to pheophytin-*a* (Chl.-*a*/Pheo.-*a*), a proxy for pigment preservation (Reuss et al., 2013), show no change in or around the period of anoxia (Fig. 4j). Zooplankton grazing is also not likely to be the main explanation for the decrease in eukaryotic algal pigments or biogenic silica. The absence of detectable pyropheophorbide-*a* between 6650 and 3500 cal yr BP indicates reduced grazing. Furthermore, consumed diatoms still contribute to sedimentary biogenic silica, and thus would be otherwise accounted for (Hobbs et al., 2010).

While mid-Holocene low-oxygen conditions in Mel3 did not favor diatoms and other eukaryotic algae, we find that cyanobacteria flourished. Despite the decline of chlorophyll-*a*, pheophytin-*a*,  $\beta$ -carotene, alloxanthin and biogenic silica, TOC in coring site A only slightly decreased during the onset of anoxia (remaining at ~2.5 wt %), indicating a compensating source of organic matter. Furthermore, while slightly lower  $\delta^{15}\text{N}$  values reflect overall reduced productivity during the anoxic period (Talbot, 2002), C/N values also reached record lows in Mel3 sediments, supporting a shift to an aquatic organic matter source. All of this evidence is consistent with the dominance of cyanobacteria, whose diagnostic pigment biomarkers persisted or increased throughout the anoxic period. Concentrations of echinenone, a pigment attributed to bulk cyanobacterial abundance (McGowan, 2007; Reuss et al., 2013), remained high at the onset of anoxia and decreased after the anoxic period ended ~3500 cal yr BP (Fig. 4e). Canthaxanthin, a pigment usually associated with colonial and often bloom-forming cyanobacteria in paleolimnological contexts, also reached peak concentrations at ~5000 cal yr BP (Fig. 4f). Moreover, canthaxanthin peaks mirror those of okenone, suggesting that similar environmental conditions favor both anoxic photosynthetic bacteria (okenone) and colonial cyanobacteria (canthaxanthin) in Mel3. This is consistent with previous observations of their coupled abundance during periods of anoxia in small, temperate lakes (e.g., Makri et al., 2019; Sanchini et al., 2020).

Cyanobacteria and the algae that produce canthaxanthin have many advantages over diatoms and green algae in harsh environments (Rebelo et al., 2020; Deshpande et al., 2014). For example, cyanobacteria are known to be vertically motile, adjusting their water column depth to account for variations in light availability and stratification, and thus dominating in systems with shallow mixed layer depths (Chung et al., 2014; J. Taylor et al., 2022). We suggest that mostly cyanobacteria and anoxic photosynthetic bacteria in Mel3 thrived in the low-oxygen environment otherwise hostile to other primary producers and grazing zooplankton from 6650 to 3500 cal yr BP. Such an observation, which has been noted in other lake systems during anoxia —e.g., in a high-elevation lake by Sorrel et al. (2021) and in a temperate lake by Żarczyński et al. (2019)— has wide-reaching implications. The observed decrease of eukaryotic primary producers in Mel3 during mid-Holocene anoxia reveals an important sensitivity of Arctic lacustrine ecosystems to oxygenation, and the absence of pyropheophorbide-*a* indicates disruption to multiple trophic levels including zooplankton. Our evidence of cyanobacterial dominance also points to the potential for bloom-forming groups to thrive in subarctic lakes when lake oxygenation declines. Many bloom-forming cyanobacteria are toxin-producing and may pose threats to drinking water sources, including in Greenland (Trout-Haney et al., 2016). This is concerning because, like many Arctic communities, nearly the whole of Greenland's population relies upon surface water (from rivers, streams, and lakes) for household water use (Gunnarsdóttir et al., 2020; Maréchal et al., 2023).

#### 4.1.4. Late-Holocene aquatic ecosystem changes post-anoxia

Concentrations of numerous pigments (chlorophyll-*a*, pheophytin-*a*,  $\beta$ -carotene, pyropheophorbide-*a*) and biogenic silica increased in sediments from both coring sites at 3500 cal yr BP, suggesting a recovery of eukaryotic primary producers and zooplankton grazing with lakewater re-oxygenation. Simultaneously, echinenone, canthaxanthin, and okenone decreased, indicating the decline of cyanobacteria and purple S bacteria post-anoxia. A second more pronounced shift in the suite of primary producers occurred at ~1200 cal yr BP, when biogenic silica and all pigments except for okenone, alloxanthin, and pyropheophorbide-*a* sharply increased, many to their highest observed levels (Fig. 4). While more complete preservation of pigments in these sediments is evidenced by higher Chl.-*a*/Pheo.-*a* ratios, there is also evidence for a real rise in primary production. Biogenic silica, which is subject to independent diagenetic processes, also increased to the second-highest levels in the entire record. Moreover, this transition is aligned with large changes in other proxies. Evidence from independent proxies for an increase in inorganic terrestrial inputs to the lake, including pulses of Ti and an increased flux of mineralogenic material, also occur at ~1200 cal yr BP; Fig. 5).

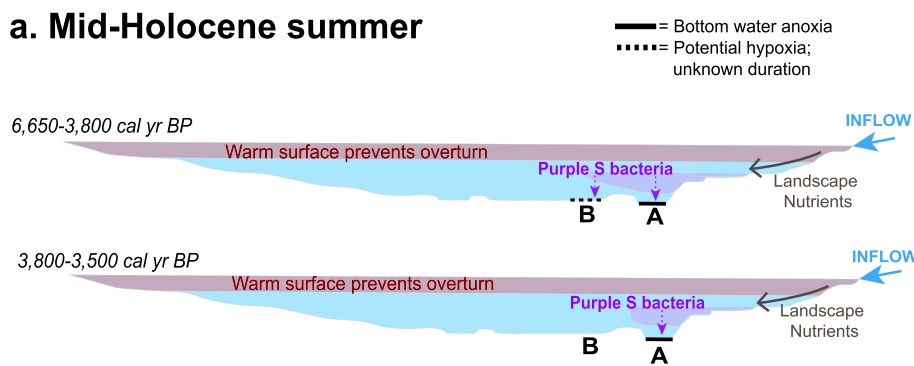
From this combination of evidence, we infer that primary productivity increases in the late-Holocene may have been driven primarily by landscape processes, with perhaps a punctuated period of higher temperatures playing a secondary role (Fig. 5). Independent paleolimnological, glaciological and modeling work indicates that climate during the late Holocene in South Greenland was characterized by low and generally declining temperatures due to progressive insolation-driven Neoglacial cooling (e.g., Andresen et al., 2004; Axford et al., 2021; Briner et al., 2016; Kaplan et al., 2002; Kaufman et al., 2009; Larocca et al., 2020; Schneider et al., 2024; Wooller et al., 2004). While lower temperatures are commonly associated with low productivity, increased input of landscape-derived materials may have provided localized nutrient-rich conditions favoring primary productivity increases in the late Holocene, particularly at 1200 cal yr BP. In addition, there may have been a period of relative warming in Medieval times as recorded in some lake sediment records (the Medieval Warm Period, 1050–550 cal yr BP, Lasher and Axford, 2019) and ice cores (~1250 cal yr BP, Buizert et al., 2018, Fig. 6). This warm period may have prolonged the interval of high primary productivity beginning at 1200 cal yr BP despite otherwise low late Holocene temperatures. A lack of intact or dateable sediments from most of the past ~500 years limits our observations of whether or not productivity experienced a decline with the end of the Medieval Warm Period, though our observations of modern ultra-oligotrophic conditions (including summer Secchi visibility to the lake bottom and abundant lake-bottom mosses) suggests a decline of primary productivity to present-day.

#### 4.2. Drivers of mid-Holocene anoxia

##### 4.2.1. Thermal stratification and climatic tipping points

There are limited studies of past oxygen conditions in Greenland lakes, but several have reconstructed protracted periods of hypolimnetic anoxia in lakes at geographically widespread locations across Greenland between ~8000 and 4000 cal yr BP. In general, reconstructed periods of hypoxia or anoxia correspond with insolation-driven, elevated (above 20th century) summer temperatures (e.g., East Greenland, Van Der Bilt et al., 2018; South Greenland, Schneider et al., 2024). McFarlin et al. (2023) describe evidence for mid-Holocene low-oxygen, methanogenic summer conditions in lakes in North, Northwest, and West Greenland, and document anoxic hypolimnetic conditions after several thousand years of prolonged relative warmth once aquatic production peaked. Mel3's anoxic period from 6650 to 3500 cal yr BP similarly occurred after a period of high (diatom) productivity (Fig. 4a) combined with elevated summer temperatures several thousand years after regional deglaciation in South Greenland (Fig. 5a, b, c), and ended as Neoglacial cooling took hold. Mechanistically, Mel3's anoxia may demonstrate how

## a. Mid-Holocene summer



## b. Late Holocene summer

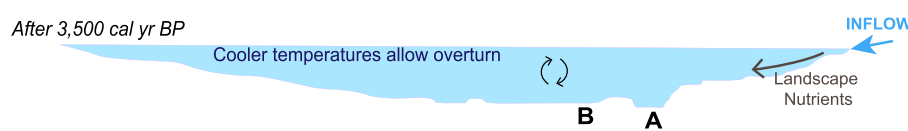


**Fig. 6. Conceptual model for drivers of anoxia at Lake Mel3.** (a) In the mid-Holocene, warmer summer temperatures promoted summer thermal stratification, and terrigenous nutrient inputs from the lake's inflow drove highest primary production and resulting propensity for anoxia near the inflow. Our records show coring site A experienced persistent bottom water anoxia (denoted by black thick lines) from 6650 to 3500 cal yr BP, whereas we capture the final stage of a hypoxic period of unknown duration terminating at 3800 cal yr BP at coring site B. (b) In the late Holocene after 3500 cal yr BP, cooling temperatures limited summer stratification and bottom waters were well oxygenated despite continuous terrigenous inputs.

warmer summer temperatures elongated the ice-free season and promoted thermal stratification that prevented wind-driven mixing for at least parts of the summer (e.g., Dibike et al., 2011; Rühland et al., 2015).

While winter stratification beneath lake ice also drives anoxia in Arctic lakes (Klanten et al., 2023; Saros et al., 2023), we argue that pigment evidence implicates summer stratification as the cause of Mel3's anoxia. Okenone is a photosynthetic pigment recording anoxic colonies of purple S bacteria during the growth season. Notably, purple S bacteria are known to require more light than other anoxigenic photosynthesizers and, even during bright summer, tend to exist at the very top of the chemocline in the anoxic zone where light availability is highest (Makri et al., 2019). At Mel3's latitude, daylight hours are short in winter (average DJF radiation = 180 MJ/m<sup>2</sup> versus JJA = 1721 MJ/m<sup>2</sup>; Cappelen and Drost Jensen, 2021), and there is thick winter snow and lake ice cover. Given the high light requirements of purple S bacteria combined with Mel3's cold-season conditions, okenone should be produced in Mel3 primarily or exclusively during the bright, ice-free growing season.

Independent regional evidence for warmer-than-present summers in the mid-Holocene in South Greenland (Larocca et al., 2020; Larsen et al., 2011; Schneider et al., 2024; Wooller et al., 2004) supports that higher warm-season surface water temperatures and consequent summer thermal stratification facilitated hypolimnetic anoxia in lake Mel3 from 6650 to 3500 cal yr BP. For example, alpine glaciers in nearby mountains of South Greenland were either absent or smaller than present from ~7100 to 3100 cal yr BP, reflecting warmer summers (Larocca et al., 2020). However, the timing and seasonality of anoxia at Mel3 contrasts with nearby lowland Lake 578, only ~17 km to the west (Schneider et al., 2024). In Lake 578, hyperspectral identification of bacteriopheophytin-e, another pigment indicative of anoxic photosynthesis derived from green S bacteria (which, unlike purple S bacteria, tolerate low-light environments), implies two earlier periods of hypolimnetic anoxia: 11,000–9600 cal yr BP and 9600–7900 cal yr BP. Schneider et al. (2024) ascribed the first to colder temperatures (indicated by sedimentary brGDGTs) that drove cool-season, under-ice stratification, and the latter to enhanced warm-season thermal stratification during the Holocene Thermal Maximum. Indicators of anoxia at Lake 578 disappeared by 5900 cal yr BP (Schneider et al., 2024), thus overlapping for <1000 years with the anoxic period we record in lake Mel3. The drivers

of anoxia are known to be complex and potentially highly localized (Klanten et al., 2023). While both lakes experienced similar regional climate influences, they are very different sites: Mel3 is at higher elevation than Lake 578 (849 m a.s.l. versus ~200 m a.s.l. respectively) and accordingly has a shorter ice-free season. The lakes have very different bathymetry, shape, watershed characteristics, nutrient inputs, and likely ecosystem dynamics throughout the Holocene, all of which can be factors driving lakewater oxygenation patterns (Klanten et al., 2023).

Overall, it is significant and important that numerous lakes across Greenland experienced periods of anoxia associated with early-to-mid-Holocene warmth (e.g., McFarlin et al., 2023; Van Der Bilt et al., 2018). In South Greenland, independent glaciological observations (Larocca et al., 2020; Larsen et al., 2011) confirm that the period of anoxia in Mel3 began ~500 years after the South Greenland ice sheet and regional mountain glaciers shrank behind their modern margins, ascribed to summer temperatures warmer than modern (Fig. 5). This summer warmth triggered a thermal tipping point that drove warm-season stratification and facilitated hypolimnetic anoxia in Mel3 and an unknown number of lakes across Greenland. However, there is considerable variation in exactly when during the Holocene Thermal Maximum other lakes developed low-oxygen conditions, both locally (Schneider et al., 2024) and in East (e.g., Ymer Lake, 5500–3000 cal yr BP; Van Der Bilt et al., 2018), North (e.g., Wax Lips Lake, 10,000–2500 cal yr BP and Trifna Sø, 7500–3000 cal yr BP; McFarlin et al., 2023) and West Greenland (Lake N3, 7500–3000 cal yr BP; McFarlin et al., 2023). It is broadly the case that in lakes across Greenland, including Mel3, anoxic conditions persisted for only part of the Holocene Thermal Maximum. This supports that higher temperatures alone have not solely driven the onset of anoxia throughout the Holocene, and that local factors (for example, in Mel3's case, increased primary production driven by terrestrial inputs, Fig. 4; Fig. 5d and e), modulate the response of lake redox states to thermal tipping points.

The tipping point that ended the anoxic period in Mel3 required persistent, millennial-scale summer cooling in the late Holocene in South Greenland and across the Arctic (Andresen et al., 2004; Axford et al., 2021; Briner et al., 2016; Kaplan et al., 2002; Kaufman et al., 2009; Larocca et al., 2020; Schneider et al., 2024; Wooller et al., 2004). Wind-mixing and oxygenation resumed as climate cooled and summer

lake stratification weakened at 3500 cal yr BP and presumably throughout the late-Holocene, when indicators of anoxia disappear from Mel3's sediments at both coring sites (Fig. 6).

#### 4.2.2. Spatial heterogeneity of anoxia and its non-climatic drivers

While seasonal water column stratification likely extended across Mel3, stratification alone does not create anoxia, and we reveal spatial inconsistency in oxygenation across Mel3's lake bottom. Okenone values, sedimentary black bands, and XRF proxies indicate that one site (coring site A) was anoxic for thousands of years, whereas the other (coring site B) may have been hypoxic for an unknown but shorter duration within that period. Horizontal variations in oxygenation have been observed in many modern small lakes across temperate and tropical regions (e.g., Crawford et al., 2015; Sadro et al., 2011; Van de Bogert et al., 2012), but similar observations from Arctic lakes are lacking (as are observations of Arctic lake oxygenation in general). Moreover, while some paleolimnological work compares sediment records from littoral versus pelagic zones (e.g., Engstrom and Rose, 2013; Taylor et al., 2015), our unique comparison between cores from two coring sites in Mel3 suggests that both deep, central coring sites were distinctly different depocenters where drivers of anoxia were highly localized.

One possible factor in explaining the greater intensity and possibly longer duration of anoxia in coring site A is that the narrow shape of the depocenter and deeper water at this core site limited wind mixing more than at site B (e.g., Deeds et al., 2021; Nürnberg, 1995), although the bathymetric differences between sites are small and we view them as unlikely to explain most of the difference in oxygen history. Another possible explanation for longer and stronger anoxia at site A is that the lake had an anoxic hypolimnion thinner than the 1 m-thick bathymetric difference between coring site A and B, i.e., a very deep chemocline that mainly affected only the deepest part of the lake (and thus only the small area directly over site A). Such a thin hypolimnion seems unlikely, and furthermore the okenone-producing purple S bacteria, which have high light requirements (Makri et al., 2019), would probably not have thrived at 12 m water depth – suggesting that the chemocline must have been shallower over coring site A. Lowered lake level could possibly allow for this pattern, making it more likely that light penetrated into a thin hypolimnion in the deepest part of the lake. However, the low abundance of benthic aquatic mosses during the anoxic period suggests that the mid-Holocene water column was not as clear as modern-day conditions at Mel3, likely due to enhanced diatom and cyanobacterial production, most likely meaning that low-oxygen habitat for purple S bacteria was not limited to the deepest waters at site A.

Instead of the explanations above, we suggest that spatial variation in Mel3's oxygenation was partly lateral and primarily driven by relative proximity to the lake inflow, which should deposit material directly into the deep and narrow coring site A. The input proximal to coring site A would have provided more terrestrially derived minerals and nutrients to enhance productivity, respiration, and subsequent anoxia at coring site A. For example, the input of P, which is known to drive cyanobacterial dominance in lakes during times of anoxia (e.g., Tu et al., 2021), was possibly elevated via surface runoff. In comparison to coring site B, we provide several lines of evidence that site A is more influenced by landscape-derived material. For instance, higher relative C/N ratios (Fig. 3e), Ti inputs and flux of overall mineralogenic material (Fig. 5d, e), and  $\delta^{13}\text{C}$  values diagnostic of a more mixed source of organic matter (Fig. 3b) throughout coring site A's Holocene record support higher terrestrial influence. The relationship between landscape inputs and anoxia has been well-documented in temperate and high-altitude settings. For example, Tu et al. (2021) found that high nutrient load in the catchment of a high-elevation Swiss lake drove high productivity, organic matter decomposition, and subsequent anoxia during stratification. Sorrel et al. (2021) found that anoxia within a stratified lake was tied to increased snowmelt, freshet, and elevated terrestrial material input, and that these coupled drivers allowed cyanobacteria to outcompete eukaryotic algae, complementing our observations in Mel3.

Makri et al. (2019) similarly found that lithogenic flux drove echinone concentrations during Holocene anoxia in a small Swiss lake, a pattern which is reflected in our finding of cyanobacterial dominance during Mel3's anoxic period amid high mineralogenic material flux and Ti input (Fig. 4; Fig. 5d and e).

Therefore, alongside climate-driven, basin-wide summer stratification across Mel3, landscape inflow may have exerted a key secondary influence on bottom waters that produced anoxia and facilitated purple S bacteria growth in coring site A from 6650 to 3500 cal yr BP, but that produced less dramatic and protracted hypoxia at the more distal site B (ending 3800 cal yr BP with an unknown onset; Fig. 6a). The importance of coupled drivers may explain why anoxia did not occur in the late Holocene, when a similar-magnitude influx of Ti, mineralogenic materials and terrestrial organic matter coincided with a primary productivity increase (~1200 cal yr BP; Fig. 5d and e), but when summer temperatures were lower and inferred thermal stratification was limited (Fig. 6b). We therefore propose that the combination of climate warming and increased nutrient inputs drove mid-Holocene anoxia observed in Mel3. As suggested elsewhere (Hessen et al., 2024), warming can decrease the nutrient input threshold required for stratification and/or ecosystem tipping points.

## 5. Conclusions & implications

The small, subarctic lake Mel3 experienced prolonged, climate-driven summer anoxia in parts of its bottom waters from 6650 to 3500 cal yr BP, and more laterally extensive hypolimnetic anoxia/hypoxia for part of that period ending at ~3800 cal yr BP. Changing oxygenation caused profound shifts in primary producer communities, including threshold changes between eukaryotic algal-dominated and cyanobacteria-dominated ecosystems. We argue that anoxia at this site was facilitated by the insolation-driven warm summer temperatures of the mid-Holocene, which promoted summer thermal stratification. At the same time, landscape processes (specifically, varying inputs of terrestrial nutrients) modulated the effects of stratification on oxygen status and drove oxygenation heterogeneity across Mel3. While our paleolimnological approach records climate-driven lake ecosystem changes over time, our results also show that single coring sites limit paleolimnological representation of important spatial biogeochemical heterogeneity in lake systems. We find that spatial heterogeneity, when reconstructed, can provide important evidence for the mechanisms that drove past environmental changes.

The causes and impacts of mid-Holocene anoxia at Mel3 provide valuable insights for the future. Our findings demonstrate how Arctic lakes' physical and chemical limnology and ecosystems can respond to temperature increases. Ongoing and future rapid anthropogenic warming in the Arctic may drive increased summer lake stratification (Dibike et al., 2011), and warming is also expected to drive coupled changes in landscape runoff (e.g., via changes in hydrologic connectivity and precipitation (Prowse et al., 2011)). Together, these predicted changes may drive widespread changes in high-latitude lake oxygenation (McFarlin et al., 2023). Furthermore, Mel3's Holocene history reveals that Arctic lakes can be susceptible to tipping points, shifting suddenly between prolonged, stable environmental states that host drastically different ecosystems. Oxygenation patterns, which exert control on species diversity, cyanobacterial abundance, water quality, and aquatic carbon cycling, are complex and are understudied in Arctic lakes (Klanten et al., 2023). As such, the need to investigate how high temperatures may have driven microbiological changes in Greenland's lakes is critical in this era of rapid Arctic warming, especially as it pertains to impacts on water resources relied upon by communities in Greenland.

## Declaration of competing interest

The authors declare no competing interests.

## Author contribution

Mia T Tuccillo: Conceptualization, Methodology, Investigation, Formal Analysis, Writing – Original Draft, Writing – Review and Editing, Visualization, Project Administration, Data Curation. Shayna C. Garla: Formal Analysis, Investigation, Data Curation. Magdalena R Osburn: Methodology, Supervision, Funding Acquisition. Bailey C Nash: Resources (e.g., sample collection). Yarrow Axford: Conceptualization, Writing – Original Draft, Writing – Review and Editing, Supervision, Project Administration, Funding Acquisition.

## Declaration of competing interest

The authors declare that they have no known competing financial interests or personal relationships that could have appeared to influence the work reported in this paper.

## Acknowledgements

This work was supported by a grant from the National Science Foundation (NSF Polar Program Award #2002515) plus internal support from Northwestern University. An NSF Doctoral Dissertation Research Improvement Grant (DDRIG, NSF Arctic System Sciences Award #2330271) additionally supported the development of pigment methods. This work would not have been possible without the people and government of Kalaallit Nunaat (Greenland) generously granting access to the field site for research, as well as field assistance from Peter Puleo, Grace Schellinger, Aidan Burdick, and Aaron Hartz, and field logistics assistance from Polarfield Services, U.S. Air National Guard, Sermeq Helicopters, and Blue Ice Adventures (Narsarsuaq, Greenland). We also acknowledge Annika Macy for assistance in radiocarbon sampling, Wesley P. Scott and Mike Lott for assistance in EA-IRMS analysis (Northwestern University Stable Isotope Laboratory and Washington State University Stable Isotope Core Laboratory, respectively), and Fernando “Ralph” Tobias for assistance with pigment methods development at the Northwestern University Integrated Molecular Structure Education and Research Center (IMSERC). MTT is especially grateful to residents of nearby Narsaq, Greenland for informative discussions about Greenland lakes, surface waters and their importance to people that have shaped the focus of this study. Finally, we gratefully acknowledge the insight of the editor and multiple anonymous reviewers, which critically improved this manuscript.

## Appendix A. Supplementary data

Supplementary data to this article can be found online at <https://doi.org/10.1016/j.quascirev.2025.109630>.

## Data availability

All data and/or code is contained within the submission.

## References

- Airs, R.L., Atkinson, J.E., Keely, B.J., 2001. Development and application of a high resolution liquid chromatographic method for the analysis of complex pigment distributions. *J. Chromatogr. A* 917 (1–2), 167–177. [https://doi.org/10.1016/S0021-9673\(01\)00663-X](https://doi.org/10.1016/S0021-9673(01)00663-X).
- Andresen, C.S., Björck, S., Bennike, O., Bond, G., 2004. Holocene climate changes in southern Greenland: evidence from lake sediments. *J. Quat. Sci.* 19 (8), 783–795. <https://doi.org/10.1002/jqs.886>.
- Antoniades, D., Veillette, J., Martineau, M.-J., Belzile, C., Tomkins, J., Pienitz, R., Lamoureux, S., Vincent, W.F., 2009. Bacterial dominance of phototrophic communities in a high Arctic lake and its implications for paleoclimate analysis. *Polar Science* 3 (3), 147–161. <https://doi.org/10.1016/j.polar.2009.05.002>.
- Axford, Y., Vernal, A. de, Osterberg, E.C., 2021. Past warmth and its impacts during the Holocene thermal maximum in Greenland. *Annu. Rev. Earth Planet Sci.* 49, 279–307. <https://doi.org/10.1146/annurev-earth-081420-063858>.
- Bouchard, F., MacDonald, L.A., Turner, K.W., Thienpont, J.R., Medeiros, A.S., Biskaborn, B.K., Korosi, J., Hall, R.I., Pienitz, R., Wolfe, B.B., 2017. Paleolimnology of thermokarst lakes: a window into permafrost landscape evolution. *Arctic Science* 3 (2), 91–117. <https://doi.org/10.1139/as-2016-0022>.
- Briner, J.P., McKay, N.P., Axford, Y., Bennike, O., Bradley, R.S., de Vernal, A., Fisher, D., Francus, P., Fréchette, B., Gajewski, K., Jennings, A., Kaufman, D.S., Miller, G., Rouston, C., Wagner, B., 2016. Holocene climate change in Arctic Canada and Greenland. *Quat. Sci. Rev.* 147, 340–364. <https://doi.org/10.1016/j.quascirev.2016.02.010>.
- Buizert, C., Keisling, B.A., Box, J.E., He, F., Carlson, A.E., Sinclair, G., DeConto, R.M., 2018. Greenland-wide seasonal temperatures during the last deglaciation. *Geophys. Res. Lett.* 45 (4), 1905–1914. <https://doi.org/10.1002/2017GL075601>.
- Burpee, B.T., Anderson, D., Saros, J.E., 2018. Assessing ecological effects of glacial meltwater on lakes fed by the Greenland Ice sheet: the role of nutrient subsidies and turbidity. *Arctic Antarct. Alpine Res.* 50 (1), S100019. <https://doi.org/10.1080/15230430.2017.1420953>.
- Cappelen, J., Drost-Jensen, C., 2021. Climatological standard normals 1991–2020 – greenland. Based on data published in DMI reports 21–12. Copenhagen. <http://www.dmi.dk/publikationer/>.
- Carlson, A.E., Winsor, K., Ullman, D.J., Brook, E.J., Rood, D.H., Axford, Y., LeGrande, A.N., Anslow, F.S., Sinclair, G., 2014. Earliest Holocene south Greenland ice sheet retreat within its late Holocene extent. *Geophys. Res. Lett.* 41 (15), 5514–5521. <https://doi.org/10.1002/2014GL060800>.
- Catalan, J., Pla-Rabés, S., Wolfe, A.P., Smol, J.P., Rühland, K.M., Anderson, N.J., Kopáček, J., Stuchlík, E., Schmidt, R., Koining, K.A., Camarero, L., Flower, R.J., Heiri, O., Kamenik, C., Korholá, A., Leavitt, P.R., Psenner, R., Renberg, I., 2013. Global change revealed by paleolimnological records from remote lakes: a review. *J. Paleolimnol.* 49 (3), 513–535. <https://doi.org/10.1007/s10933-013-9681-2>.
- Chung, S.W., Imberger, J., Hipsey, M.R., Lee, H.S., 2014. The influence of physical and physiological processes on the spatial heterogeneity of a *Microcystis* bloom in a stratified reservoir. *Ecol. Model.* 289, 133–149. <https://doi.org/10.1016/j.ecolmodel.2014.07.010>.
- Crawford, J.T., Loken, L.C., Casson, N.J., Smith, C., Stone, A.G., Winslow, L.A., 2015. High-speed limnology: using advanced sensors to investigate spatial variability in biogeochemistry and hydrology. *Environ. Sci. Technol.* 49 (1), 442–450. <https://doi.org/10.1021/es504773x>.
- Davison, W., 1993. Iron and manganese in lakes. *Earth Sci. Rev.* 34 (2), 119–163. [https://doi.org/10.1016/0012-8252\(93\)90029-7](https://doi.org/10.1016/0012-8252(93)90029-7).
- Deeds, J., Amirbahman, A., Norton, S.A., Suitor, D.G., Bacon, L.C., 2021. Predicting anoxia in low-nutrient temperate lakes. *Ecol. Appl.* 31 (6), e02361. <https://doi.org/10.1002/ea.2361>.
- Deshpande, B.N., Maps, F., Matveev, A., Vincent, W.F., 2017. Oxygen depletion in subarctic peatland thaw lakes. *Arctic Science* 3 (2), 406–428. <https://doi.org/10.1139/as-2016-0048>.
- Deshpande, B.N., Tremblay, R., Pienitz, R., Vincent, W.F., 2014. Sedimentary pigments as indicators of cyanobacterial dynamics in a hyper-eutrophic lake. *J. Paleolimnol.* 52 (3), 171–184. <https://doi.org/10.1007/s10933-014-9785-3>.
- Dibike, Y., Prowse, T., Saloranta, T., Ahmed, R., 2011. Response of northern hemisphere lake ice cover and lake-water thermal structure patterns to a changing climate. *Hydrocl. Process.* 25 (19), 2942–2953. <https://doi.org/10.1002/hyp.8068>.
- Dreßler, M., Hübener, T., Görs, S., Werner, P., Selig, U., 2007. Multi-proxy reconstruction of trophic state, hypolimnetic anoxia and phototrophic sulphur bacteria abundance in a dimictic Lake in Northern Germany over the past 80 years. *J. Paleolimnol.* 37 (2), 205–219. <https://doi.org/10.1007/s10933-006-9013-x>.
- Engstrom, D.R., Rose, N.L., 2013. A whole-basin, mass-balance approach to paleolimnology. *J. Paleolimnol.* 49 (3), 333–347. <https://doi.org/10.1007/s10933-012-9675-5>.
- Florian, C.R., Miller, G.H., Fogel, M.L., Wolfe, A.P., Vinebrooke, R.D., Geirsdóttir, Á., 2015. Algal pigments in Arctic lake sediments record biogeochemical changes due to Holocene climate variability and anthropogenic global change. *J. Paleolimnol.* 54 (1), 53–69. <https://doi.org/10.1007/s10933-015-9835-5>.
- Fréchette, B., de Vernal, A., 2009. Relationship between Holocene climate variations over southern Greenland and eastern Baffin Island and synoptic circulation pattern. *Clim. Past* 5 (3), 347–359. <https://doi.org/10.5194/cp-5-347-2009>.
- Fritz, S.C., Anderson, N.J., 2013. The relative influences of climate and catchment processes on Holocene lake development in glaciated regions. *J. Paleolimnol.* 49 (3), 349–362. <https://doi.org/10.1007/s10933-013-9684-z>.
- Fulton, J.M., Arthur, M.A., Thomas, B., Freeman, K.H., 2018. Pigment carbon and nitrogen isotopic signatures in euxinic basins. *Geobiology* 16 (4), 429–445. <https://doi.org/10.1111/gbi.12285>.
- Gunnarsdóttir, M.J., Gardarsson, S.M., Schultz, A.C., Albrechtsen, H.-J., Hansen, L.T., Gerlach Bergkvist, K.S., Rossi, P.M., Klöve, B., Myrmeal, M., Persson, K.M., Eriksson, M., Bartram, J., 2020. Status of risk-based approach and national framework for safe drinking water in small water supplies of the nordic water sector. *Int. J. Hyg Environ. Health* 230, 113627. <https://doi.org/10.1016/j.ijheh.2020.113627>.
- Harradine, P.J., Harris, P.G., Head, R.N., Harris, R.P., Maxwell, J.R., 1996. Steryl chlorin esters are formed by zooplankton herbivory. *Geochim. Cosmochim. Acta* 60 (12), 2265–2270. [https://doi.org/10.1016/0016-7037\(96\)00132-9](https://doi.org/10.1016/0016-7037(96)00132-9).
- Hessen, D.O., Andersen, T., Armstrong McKay, D., Kosten, S., Meerhoff, M., Pickard, A., Spears, B.M., 2024. Lake ecosystem tipping points and climate feedbacks. *Earth Syst. Dyn.* 15 (3), 653–669. <https://doi.org/10.5194/esd-15-653-2024>.
- Hobbs, W.O., Telford, R.J., Birks, H.J.B., Saros, J.E., Hazewinkel, R.R.O., Perren, B.B., Saulnier-Talbot, É., Wolfe, A.P., 2010. Quantifying recent ecological changes in remote Lakes of North America and Greenland using sediment diatom assemblages. *PLoS One* 5 (4), e10026. <https://doi.org/10.1371/journal.pone.0010026>.

- Itoh, N., Tani, Y., Soma, Y., Soma, M., 2007. Accumulation of sedimentary photosynthetic pigments characterized by pyrophorophorbide a and sterol chlorin esters (SCEs) in a shallow eutrophic coastal lake (Lake Hamana, Japan). *Estuar. Coast Shelf Sci.* 71 (1–2), 287–300. <https://doi.org/10.1016/j.ecss.2006.07.019>.
- Jeffrey, S.W., Veske, M., 1997. Introduction to marine phytoplankton and their pigment signatures. In: Jeffrey, S.W., Mantoura, R.F.C., Wright, S.W. (Eds.), *Phytoplankton Pigments in Oceanography: Guidelines to Modern Methods*, vol. 10. UNESCO Publishing, Paris, pp. 74–75.
- Jeppesen, E., Davidson, T.A., Meerhoff, M., De Meester, L., González-Bergonzoni, I., Vidal, N., Arndt, H., Jürgens, K., Sommaruga, R., Özkan, K., Lauridsen, T.L., Tserenpil, S., 2023. Differences in food web structure and composition between new and nearby older lakes in West Greenland suggest succession trajectories driven by glacier retreat. *Hydrobiologia* 850 (21), 4745–4761. <https://doi.org/10.1007/s10750-023-05189-4>.
- Kaplan, M.R., Wolfe, A.P., Miller, G.H., 2002. Holocene environmental variability in Southern Greenland inferred from Lake sediments. *Quat. Res.* 58 (2), 149–159. <https://doi.org/10.1006/qres.2002.2352>.
- Kaufman, D.S., Schneider, D.P., McKay, N.P., Ammann, C.M., Bradley, R.S., Briffa, K.R., Miller, G.H., Otto-Bliesner, B.L., Overpeck, J.T., Vinther, B.M., Arctic Lakes 2k Project Members, Abbott, M., Axford, Y., Bird, B., Birks, H.J.B., Bjune, A.E., Briner, J., Cook, T., Chipman, M., et al., 2009. Recent warming reverses long-term Arctic cooling. *Science* 325 (5945), 1236–1239. <https://doi.org/10.1126/science.1173983>.
- Kirillin, G., Leppäpäärtti, M., Terzhevskii, A., Granin, N., Bernhardt, J., Engelhardt, C., Efremova, T., Golosov, S., Palshin, N., Sherstyankin, P., Zdrovovenova, G., Zdrovovenov, R., 2012. Physics of seasonally ice-covered lakes: a review. *Aquat. Sci.* 74 (4), 659–682. <https://doi.org/10.1007/s00027-012-0279-y>.
- Klanton, Y., Couture, R.-M., Christoffersen, K.S., Vincent, W.F., Antoniades, D., 2023. Oxygen depletion in Arctic Lakes: circumpolar trends, biogeochemical processes, and implications of climate change. *Glob. Biogeochem. Cycles* 37 (5), e2022GB007616. <https://doi.org/10.1029/2022GB007616>.
- Larocca, L.J., Axford, Y., Björk, A.A., Lasher, G.E., Brooks, J.P., 2020. Local glaciers record delayed peak Holocene warmth in south Greenland. *Quat. Sci. Rev.* 241, 106421. <https://doi.org/10.1016/j.quascirev.2020.106421>.
- Larsen, N.K., Kjær, K.H., Olsen, J., Funder, S., Kjeldsen, K.K., Nørgaard-Pedersen, N., 2011. Restricted impact of Holocene climate variations on the southern Greenland Ice Sheet. *Quat. Sci. Rev.* 30 (21), 3171–3180. <https://doi.org/10.1016/j.quascirev.2011.07.022>.
- Lasher, G.E., Axford, Y., 2019. Medieval warmth confirmed at the Norse Eastern Settlement in Greenland. *Geology* 47 (3), 267–270. <https://doi.org/10.1130/G45833.1>.
- Leavitt, P.R., Findlay, D.L., 1994. Comparison of fossil pigments with 20 years of phytoplankton data from Eutrophic Lake 227, experimental Lakes area, Ontario. *Can. J. Fish. Aquat. Sci.* 51 (10), 2286–2299. <https://doi.org/10.1139/F94-232>.
- Leavitt, P.R., Hodgson, D.A., 2002. Sedimentary pigments. In: Smol, J.P., Birks, H.J.B., Last, W.M., Bradley, R.S., Alverson, K. (Eds.), *Tracking Environmental Change Using Lake Sediments*, vol. 3. Springer, Netherlands, pp. 295–325. [https://doi.org/10.1007/0-306-47668-1\\_15](https://doi.org/10.1007/0-306-47668-1_15).
- Makri, S., Lami, A., Lods-Crochet, B., Loizeau, J.-L., 2019. Reconstruction of trophic state shifts over the past 90 years in a eutrophicated lake in western Switzerland, inferred from the sedimentary record of photosynthetic pigments. *J. Paleolimnol.* 61 (2), 129–145. <https://doi.org/10.1007/s10933-018-0049-5>.
- Maréchal, J.Y.A., Hansen, L.T., Jensen, P.E., 2023. Water quality in rural Greenland—Acceptability and safety. *Hyg. Environ. Heal.* 7, 100065. <https://doi.org/10.1016/j.heha.2023.100065>.
- Massa, C., Perren, B.B., Gauthier, É., Bichet, V., Petit, C., Richard, H., 2012. A multiproxy evaluation of Holocene environmental change from Lake Igalliku, South Greenland. *J. Paleolimnol.* 48 (1), 241–258. <https://doi.org/10.1007/s10933-012-9594-5>.
- McFarlin, J.M., Axford, Y., Kusch, S., Masterson, A.L., Lasher, G.E., Osburn, M.R., 2023. Aquatic plant wax hydrogen and carbon isotopes in Greenland lakes record shifts in methane cycling during past Holocene warming. *Sci. Adv.* 9 (39), eadh9704. <https://doi.org/10.1126/sciadv.adh9704>.
- McGowan, S., 2007. *Pigment Studies*. Elsevier, pp. 2062–2074. <https://doi.org/10.1016/B0-444-52747-8/00247-7>.
- McGowan, S., Anderson, N.J., Edwards, M.E., Hopla, E., Jones, V., Langdon, P.G., Law, A., Solovieva, N., Turner, S., Van Hardenbroek, M., Whiteford, E.J., Wiik, E., 2018. Vegetation transitions drive the autotrophy-heterotrophy balance in Arctic lakes. *Limnology and Oceanography Letters* 3 (3), 246–255. <https://doi.org/10.1002/lo.10086>.
- Mewafy, F.M., Atekwana, E.A., Werkema, D.D., Slater, L.D., Ntarlagiannis, D., Revil, A., Skold, M., Delin, G.N., 2011. Magnetic susceptibility as a proxy for investigating microbially mediated iron reduction: MS as proxy for iron reduction. *Geophys. Res. Lett.* 38 (21). <https://doi.org/10.1029/2011GL049271> n/a-n/a.
- Meyers, P.A., 1994. Preservation of elemental and isotopic source identification of sedimentary organic matter. *Chem. Geol.* 114 (3), 289–302. [https://doi.org/10.1016/0009-2541\(94\)90059-0](https://doi.org/10.1016/0009-2541(94)90059-0).
- Mortlock, R.A., Froelich, P.N., 1989. A simple method for the rapid determination of biogenic opal in pelagic marine sediments. *Deep-Sea Res., Part A* 36 (9), 1415–1426. [https://doi.org/10.1016/0198-0149\(89\)90092-7](https://doi.org/10.1016/0198-0149(89)90092-7).
- Myers-Smith, I.H., Kerby, J.T., Phoenix, G.K., Bjerke, J.W., Epstein, H.E., Assmann, J.J., John, C., Andreu-Hayles, L., Angers-Blondin, S., Beck, P.S.A., Berner, L.T., Bhatt, U. S., Bjorkman, A.D., Blok, D., Bryn, A., Christiansen, C.T., Cornelissen, J.H.C., Cunliffe, A.M., Elmendorf, S.C., et al., 2020. Complexity revealed in the greening of the Arctic. *Nat. Clim. Change* 10 (2), 106–117. <https://doi.org/10.1038/s41558-019-0688-1>.
- Nelson, A.H., Bierman, P.R., Shakun, J.D., Rood, D.H., 2014. Using in situ cosmogenic  $^{10}\text{Be}$  to identify the source of sediment leaving Greenland. *Earth Surf. Process. Landf.* 39 (8), 1087–1100. <https://doi.org/10.1002/esp.3565>.
- Nürnberg, G.K., 1995. Quantifying anoxia in lakes. *Limnol. Oceanogr.* 40 (6), 1100–1111. <https://doi.org/10.4319/lo.1995.40.6.1100>.
- Olsen, J., Anderson, N.J., Knudsen, M.F., 2012. Variability of the North Atlantic oscillation over the past 5,200 years. *Nat. Geosci.* 5 (11), 808–812. <https://doi.org/10.1038/ngeo1589>.
- Perren, B.B., Bradley, R.S., Francus, P., 2003. Rapid lacustrine response to recent high arctic warming: a diatom record from Sawtooth Lake, Ellesmere Island, Nunavut. *Arctic Antarct. Alpine Res.* 35 (3), 271–278. [https://doi.org/10.1657/1523-0430\(2003\)035\[0271:RLTRH\]2.0.CO;2](https://doi.org/10.1657/1523-0430(2003)035[0271:RLTRH]2.0.CO;2).
- Perren, B.B., Wolfe, A.P., Cooke, C.A., Kjær, K.H., Mazzucchi, D., Steig, E.J., 2012. Twentieth-century warming revives the world's northernmost lake. *Geology* 40 (11), 1003–1006. <https://doi.org/10.1130/G33621.1>.
- Phoenix, G.K., Bjerke, J.W., 2016. Arctic browning: extreme events and trends reversing Arctic greening. *Glob. Change Biol.* 22 (9), 2960–2962. <https://doi.org/10.1111/gcb.13261>.
- Prater, C., Bullard, J.E., Osburn, C.L., Martin, S.L., Watts, M.J., Anderson, N.J., 2022. Landscape controls on nutrient stoichiometry regulate lake primary production at the margin of the Greenland ice sheet. *Ecosystems* 25 (4), 931–947. <https://doi.org/10.1007/s10021-021-00693-x>.
- Pribyl, D.W., 2010. A critical review of the conventional SOC to SOM conversion factor. *Geoderma* 156 (3), 75–83. <https://doi.org/10.1016/j.geoderma.2010.02.003>.
- Prowse, T., Alfreiden, K., Beltaos, S., Bonsal, B.R., Bowden, W.B., Duguay, C.R., Korholo, A., McNamara, J., Vincent, W.F., Vuglinsky, V., Walter Anthony, K.M., Weyhenmeyer, G.A., 2011. Effects of changes in Arctic lake and river ice. *Ambio* 40 (1), 63–74. <https://doi.org/10.1007/s13280-011-0217-6>.
- Puleo, P.J.K., Axford, Y., 2023. Duration and ice thickness of a late Holocene outlet glacier advance near Narsarsuaq, southern Greenland. *Clim. Past* 19 (9), 1777–1791. <https://doi.org/10.5194/cp-19-1777-2023>.
- Rantanen, M., Karpechko, A.Y., Lipponen, A., Nordling, K., Hyvärinen, O., Ruosteenoja, K., Vihamäki, T., Laaksonen, A., 2022. The Arctic has warmed nearly four times faster than the globe since 1979. *Commun. Earth Environ.* 3 (1), 1–10. <https://doi.org/10.1038/s43247-022-00498-3>.
- Rebelo, B.A., Farrona, S., Ventura, M.R., Abranched, R., 2020. Canthaxanthin, a red-hot carotenoid: applications, synthesis, and biosynthetic evolution. *Plants* 9 (8), 1039. <https://doi.org/10.3390/plants9081039>.
- Reimer, P.J., Austin, W.E.N., Bard, E., Bayliss, A., Blackwell, P.G., Ramsey, C.B., Butzin, M., Cheng, H., Edwards, R.L., Friedrich, M., Grootes, P.M., Guilderson, T.P., Hajdas, I., Heaton, T.J., Hogg, A.G., Hughen, K.A., Kromer, B., Manning, S.W., Muscheler, R., et al., 2020. The IntCal20 Northern Hemisphere radiocarbon Age calibration curve (0–55 cal kBP). *Radiocarbon* 62 (4), 725–757. <https://doi.org/10.1017/RDC.2020.41>.
- Reuss, N.S., Anderson, N.J., Fritz, S.C., Simpson, G.L., 2013. Responses of microbial phototrophs to late-holocene environmental forcing of lakes in south-west Greenland. *Freshw. Biol.* 58 (4), 690–704. <https://doi.org/10.1111/fwb.12073>.
- Rühland, K.M., Paterson, A.M., Smol, J.P., 2015. Lake diatom responses to warming: reviewing the evidence. *J. Paleolimnol.* 54 (1), 1–35. <https://doi.org/10.1007/s10933-015-9837-3>.
- Rühland, K., Paterson, A.M., Smol, J.P., 2008. Hemispheric-scale patterns of climate-related shifts in planktonic diatoms from North American and European lakes. *Glob. Change Biol.* 14 (11), 2740–2754. <https://doi.org/10.1111/j.1365-2486.2008.01670.x>.
- Sadro, S., Melack, J.M., MacIntyre, S., 2011. Spatial and temporal variability in the ecosystem metabolism of a high-elevation lake: integrating benthic and pelagic habitats. *Ecosystems* 14 (7), 1123–1140. <https://doi.org/10.1007/s10021-011-9471-5>.
- Sanchini, A., Szidat, S., Tylmann, W., Vogel, H., Wacnik, A., Grosjean, M., 2020. A Holocene high-resolution record of aquatic productivity, seasonal anoxia and meromixis from varved sediments of Lake Łazduny, North-Eastern Poland: insight from a novel multi-proxy approach. *J. Quat. Sci.* 35 (8), 1070–1080. <https://doi.org/10.1002/jqs.3242>.
- Saros, J.E., Anderson, N.J., Juggins, S., McGowan, S., Yde, J.C., Telling, J., Bullard, J.E., Yallow, M.L., Heathcote, A.J., Burpee, B.T., Fowler, R.A., Barry, C.D., Northington, R.M., Osburn, C.L., Pla-Rabes, S., Mernild, S.H., Whiteford, E.J., Andrews, M.G., Kerby, J.T., Post, E., 2019. Arctic climate shifts drive rapid ecosystem responses across the West Greenland landscape. *Environ. Res. Lett.* 14 (7), 074027. <https://doi.org/10.1088/1748-9326/ab2928>.
- Saros, J.E., Arp, C.B., Bouchard, F., Comte, J., Couture, R.-M., Dean, J.F., Lafrenière, M., MacIntyre, S., McGowan, S., Rautio, M., Prater, C., Tank, S.E., Walvoord, M., Wicklund, K.P., Antoniades, D., Ayala-Borda, P., Canario, J., Drake, T.W., Folhas, D., et al., 2023. Sentinel responses of Arctic freshwater systems to climate: linkages, evidence, and a roadmap for future research. *Arctic Science* 9 (2), 356–392. <https://doi.org/10.1038/as-2022-0021>.
- Saros, J.E., Northington, R.M., Osburn, C.L., Burpee, B.T., John Anderson, N., 2016. Thermal stratification in small Arctic lakes of southwest Greenland affected by water transparency and epilimnetic temperatures. *Limnol. Oceanogr.* 61 (4), 1530–1542. <https://doi.org/10.1002/lno.10314>.
- Schartau, A.K., Mariash, H.L., Christoffersen, K.S., Bogan, D., Dubovskaya, O.P., Fefilova, E.B., Hayden, B., Ingavson, H.R., Ivanova, E.A., Kononova, O.N., Kravchuk, E.S., Lento, J., Majaneva, M., Novichkova, A.A., Rautio, M., R\_hland, K.M., Shaftel, R., Smol, J.P., Vrede, T., Kahlilainen, K.K., 2022. First circumpolar assessment of Arctic freshwater phytoplankton and zooplankton diversity: spatial patterns and environmental factors. *Freshw. Biol.* 67 (1), 141–158. <https://doi.org/10.1111/fwb.13783>.

- Schneider, T., Castañeda, I.S., Zhao, B., Krüger, S., Salacup, J.M., Bradley, R.S., 2024. Tracing Holocene temperatures and human impact in a Greenlandic Lake: novel insights from hyperspectral imaging and lipid biomarkers. *Quat. Sci. Rev.* 339, 108851. <https://doi.org/10.1016/j.quascirev.2024.108851>.
- Smol, J.P., 1983. Paleophycology of a high Arctic lake near cape Herschel, Ellesmere Island. *Can. J. Bot.* 61 (8), 2195–2204. <https://doi.org/10.1139/b83-238>.
- So, R.T., Blair, N.E., Masterson, A.L., 2020. Carbonate mineral identification and quantification in sediment matrices using diffuse reflectance infrared Fourier transform spectroscopy. *Environ. Chem. Lett.* 18 (5), 1725–1730. <https://doi.org/10.1007/s10311-020-01027-4>.
- Sorrel, P., Jacq, K., Van Exem, A., Escarguel, G., Dietre, B., Debret, M., McGowan, S., Ducept, J., Gauthier, E., Oberhänsli, H., 2021. Evidence for centennial-scale mid-holocene episodes of hypolimnetic anoxia in a high-altitude lake system from central Tian Shan (Kyrgyzstan). *Quat. Sci. Rev.* 252, 106748. <https://doi.org/10.1016/j.quascirev.2020.106748>.
- Squier, A.H., Hodgson, D.A., Keely, B.J., 2002. Sedimentary pigments as markers for environmental change in an Antarctic lake. *Org. Geochem.* 33 (12), 1655–1665. [https://doi.org/10.1016/S0146-6380\(02\)00177-8](https://doi.org/10.1016/S0146-6380(02)00177-8).
- Stevenson, M.A., McGowan, S., Pearson, E.J., Swann, G.E.A., Leng, M.J., Jones, V.J., Bailey, J.J., Huang, X., Whiteford, E., 2021. Anthropocene climate warming enhances autochthonous carbon cycling in an upland Arctic lake, Disko Island, West Greenland. *Biogeosciences* 18 (8), 2465–2485. <https://doi.org/10.5194/bg-18-2465-2021>.
- Stuiver, M., Reimer, P.J., Reimer, R.W., 2022. Calib 8.2 [WWW program] at. <http://calib.org>, 30-2.
- Talbot, M.R., 2002. Nitrogen isotopes in palaeolimnology. In: Last, W.M., Smol, J.P. (Eds.), *Tracking Environmental Change Using Lake Sediments*, vol. 2. Springer, Netherlands, pp. 401–439. [https://doi.org/10.1007/0-306-47670-3\\_15](https://doi.org/10.1007/0-306-47670-3_15).
- Taylor, J., Calderer, M.C., Hondzo, M., Voller, V.R., 2022. A theoretical modeling framework for motile and colonial harmful algae. *Ecol. Evol.* 12 (7), e9042. <https://doi.org/10.1002/ece3.9042>.
- Taylor, Z.P., Horn, S.P., Finkelstein, D.B., 2015. Assessing intra-basin spatial variability in geochemical and isotopic signatures in the sediments of a small neotropical lake. *J. Paleolimnol.* 54 (4), 395–411. <https://doi.org/10.1007/s10933-015-9859-x>.
- Trout-Haney, J., Wood, Z., Cottingham, K., 2016. Presence of the Cyanotoxin Microcystin in Arctic Lakes of Southwestern Greenland. *Toxins* 8 (9), 256. <https://doi.org/10.3390/toxins8090256>.
- Tu, L., Gilli, A., Lotter, A.F., Vogel, H., Moyle, M., Boyle, J.F., Grosjean, M., 2021. The nexus among long-term changes in lake primary productivity, deep-water anoxia, and internal phosphorus loading, explored through analysis of a 15,000-year varved sediment record. *Global Planet. Change* 207, 103643. <https://doi.org/10.1016/j.gloplacha.2021.103643>.
- Upton, B.G.J., Emeleus, C.H., Heaman, L.M., Goodenough, K.M., Finch, A.A., 2003. Magmatism of the mid-Proterozoic Gardar Province, South Greenland: chronology, petrogenesis and geological setting. *Lithos* 68 (1), 43–65. [https://doi.org/10.1016/S0024-4937\(03\)00030-6](https://doi.org/10.1016/S0024-4937(03)00030-6).
- Van de Bogert, M.C., Bade, D.L., Carpenter, S.R., Cole, J.J., Pace, M.L., Hanson, P.C., Langman, O.C., 2012. Spatial heterogeneity strongly affects estimates of ecosystem metabolism in two north temperate lakes. *Limnol. Oceanogr.* 57 (6), 1689–1700. <https://doi.org/10.4319/lo.2012.57.6.1689>.
- Van Der Bilt, W.G.M., Rea, B., Spagnolo, M., Roerdink, D.L., Jørgensen, S.L., Bakke, J., 2018. Novel sedimentological fingerprints link shifting depositional processes to Holocene climate transitions in East Greenland. *Global Planet. Change* 164, 52–64. <https://doi.org/10.1016/j.gloplacha.2018.03.007>.
- Vincent, W.F., Quesada, A., 2012. Cyanobacteria in high latitude Lakes, Rivers and Seas. In: Whitton, B.A. (Ed.), *Ecology of Cyanobacteria II*. Springer, Netherlands, pp. 371–385. [https://doi.org/10.1007/978-94-007-3855-3\\_13](https://doi.org/10.1007/978-94-007-3855-3_13).
- Wolfe, A.P., Cooke, C.A., Hobbs, W.O., 2006. Are current rates of atmospheric nitrogen deposition influencing Lakes in the Eastern Canadian arctic? *Arctic Antarct. Alpine Res.* 38 (3), 465–476. [https://doi.org/10.1657/1523-0430\(2006\)38\[465:ACROAN\]2.0.CO;2](https://doi.org/10.1657/1523-0430(2006)38[465:ACROAN]2.0.CO;2).
- Woulds, C., Cowie, G.L., 2009. Sedimentary pigments on the Pakistan margin: controlling factors and organic matter dynamics. *Deep Sea Res. Part II Top. Stud. Oceanogr.* 56 (6–7), 347–357. <https://doi.org/10.1016/j.dsro.2008.05.033>.
- Żarczyński, M., Wacnik, A., Tylmann, W., 2019. Tracing lake mixing and oxygenation regime using the Fe/Mn ratio in varved sediments: 2000 year-long record of human-induced changes from Lake Żabińskie (NE Poland). *Sci. Total Environ.* 657, 585–596. <https://doi.org/10.1016/j.scitotenv.2018.12.078>.